Ocean Engineering 243 (2022) 110186

Contents lists available at ScienceDirect

Ocean Engineering

journal homepage: www.elsevier.com/locate/oceaneng

A rational model for maneuvering in irregular waves with the effect of waves on the propeller and rudder inflow taken into account

Øyvind Rabliås *, Trygve Kristiansen

Department of Marine Technology, NTNU, 7491, Trondheim, Norway

ARTICLE INFO

Keywords:
Maneuvering in irregular waves
Turning circles
Wave effects on the rudder
Free running experiments

ABSTRACT

A modular model for maneuvering in regular and irregular waves is presented. A new model is presented for the y-component of the rudder inflow. Moreover, an efficient time-domain method for estimation of slowly varying drift loads in irregular waves is presented. Simulations of turning circles in irregular waves with the time-domain method, are compared to simulations where the difference-frequency loads, with the Newman approximation, is used to estimate the slowly varying drift loads. These two methods show similar accuracy, but the time-domain method is significantly faster. The numerical simulations are compared with new free running experiments of the Duisburg Test Case (DTC). Based on extensive wave documentation in the Ocean basin at SINTEF Ocean, the uncertainty in maneuvering experiments, due to variation of wave height throughout the basin, is investigated. The uncertainty is not insignificant, but it is less than expected. The sensitivity to number of realizations in the same irregular wave spectrum is investigated, both experimental and numerical. For some responses, up to 20 repetitions are needed before the width of the 95% confidence intervals approach convergence.

1. Introduction

Maneuvering in waves has received increasing attention the last decades. The main focus has been on maneuvering in regular waves. Based on a two-time scale assumption, Skejic and Faltinsen (2006) presented a modular maneuvering model for maneuvering in regular waves. The assumption is that the slowly varying maneuvering motions have a more slowly varying time scale than the linear wave induced motions. Hence, the dominating contribution to the maneuvering motion from regular waves is the second-order drift loads. This two-time scale assumption is used by several other authors, e.g. Yasukawa and Nakayama (2009), Seo and Kim (2011), Zhang and Zou (2016), Cura-Hochbaum and Uharek (2016), Chillcce and el Moctar (2018), and Yu et al. (2021). The models mentioned above are based on different frameworks, the one thing in common is that the effects of regular waves are accounted for by the second-order drift loads only, i.e. the rest of the hydrodynamic loads on the ship are calculated as for calm water. In Rabliås and Kristiansen (2021) the authors' of the present paper, applied the two-scale assumption in a modular maneuvering model, to simulate turning circles with 35° rudder angle, of the Duisburg Test Case (DTC), for a range of wavelengths, with satisfactory accuracy.

In ship maneuvering in deep water, there is a consensus that the slowly varying drift loads are the most dominating contribution from waves. This is exemplified by the high accuracy of the models above (and other models using this approach). However, this does not exclude that the waves can affect other modules of the maneuvering model, e.g. the propeller thrust and rudder loads. Moreover, the two-time scale assumption can be questionable for long waves, in particular for following sea. This is because when the encounter wave frequency is low, the linear wave induced motions can experience the same time-scale as the maneuvering motion.

Seo et al. (2019) compared numerical simulations of turning circles, in regular and irregular waves, where the drift loads were accounted for, with experiments. They suspected that one of the reasons to the discrepancy from experiments, for the longest waves, was because the effects of waves on rudder and propulsion was ignored. Wang et al. (2018) investigated surf-riding and broaching, where propeller and rudder immersion due to waves were accounted for. They concluded that rudder immersion is the key factor for the emergence of broaching motions. Aung and Umeda (2020) investigated, with a modular maneuvering model, the sensitivity of rudder and propeller emergence in adverse weather conditions. The velocity was not significantly affected, while the trajectory was affected by the rudder and propeller emergence. Nguyen et al. (2018) investigated, with CFD, the effects of regular waves on the rudder forces, for five different wave headings

* Corresponding author.
E-mail address: oyvind.rablias@ntnu.no (Ø. Rabliås).

https://doi.org/10.1016/j.oceaneng.2021.110186
Received 22 June 2021; Received in revised form 8 November 2021; Accepted 9 November 2021
Available online 4 December 2021
0029-8018/© 2021 The Authors. Published by Elsevier Ltd. This is an open access article under the CC BY license (http://creativecommons.org/licenses/by/4.0/).

and a range of wavelengths, λ/L = 0.4–2. Their results indicated a significant influence on the rudder lift and drag, in particular for the longest waves. Tello Ruiz et al. (2019) investigated experimentally, for wavelengths λ/L = 0.2–0.8, the effects of waves on the rudder loads. Their results indicated that the effect of waves, for the tested conditions, on the propeller and rudder were negligible. However, only head sea and following sea were tested, and the wave amplitudes were moderate.

Nakamura and Naito (1975) showed that the wake velocities fluctuate due to waves and ship motions, and the mean of the fluctuations differs from the calm water wake. Furthermore, their experiments indicated that the pitch motion was the dominating cause to the change in wake. Faltinsen et al. (1980) proposed a wake model that accounts for the increase in mean propeller inflow due to wave induced pitch motion. Ueno et al. (2013) presented a method for the fluctuating part of the wake velocity. Taskar et al. (2016) combined the two methods above, and presented a method that takes into account both the change in mean wake and the fluctuating part. The wave modified wake, affects the propeller inflow velocity, as well as the x-component of the rudder inflow. However, there is no one, in the authors' knowledge, that has presented a model for the y-component of the wave modified rudder inflow.

For maneuvering in a seaway, there is done less research compared to maneuvering in regular waves. Skejic and Faltinsen (2013) used the Newman approximation, with random phase angles, to calculate the second-order difference-frequency loads, i.e. the slowly varying drift loads. They simulated, with a modular maneuvering model, turning circles in irregular waves. Yasukawa et al. (2018) simulated turning circles in irregular waves, where only the steady average force was accounted for, i.e. the stochastic behavior was not accounted for. Both methods above use a wave spectrum for an irregular sea state, and calculate the drift loads for each component in the spectrum with the same numerical method as for regular waves. For the average loads, a single sum is computed for each time instants the drift loads are calculated. For the difference-frequency loads, in principle it is necessary to compute a double sum, which is computationally demanding. It is possible to approximate the double sum to a single sum, which will reduce the computational cost somewhat. However, even the single sum can be computationally demanding, meaning that the time needed to perform a simulation in irregular waves is significantly higher compared to regular waves.

If a maneuver is repeated in an irregular sea state, the trajectory and velocities will not be identical for different repetitions. This is due to the stochastic variation of the wave elevation in an irregular sea state. The stochastic behavior is not accounted for if only the averaged second-order drift loads are accounted for. Seo et al. (2019) simulated turning circles in irregular waves, where the second-order difference-frequency loads, with random phase angles, were accounted for. They investigated the sensitivity of different time realizations in the same wave spectrum, for drifting distance and drifting angle. Their results indicated that the variation around the mean converged after 15 repetitions.

In the present work, the modular maneuvering model in Rabliås and Kristiansen (2021) is further developed. The drift loads in regular waves are calculated with a new approach, where the added resistance (x-drift) is calculated with the same strip-theory as in Rabliås and Kristiansen (2021), while the y- and yaw-drift are calculated with a 3D panel code with no forward speed effects. This is similar to the approach presented in Yasukawa et al. (2018). This is justified by the fact that the forward speed has only a small effect on the y- and yaw-drift. A new model is presented for the rudder inflow. The x-component of the inflow is calculated with the model in Taskar et al. (2016), while the y-component of the inflow is derived consistently to account for the same effects as the x-component. The slowly varying drift loads in irregular waves are calculated with two different methods, the difference-frequency loads using the Newman approximation, and a "time-domain" method where the incident wave elevation is decomposed into a series of individual waves. The time-domain method was first presented by Hsu and Blenkarn (1972), and it is fundamentally different to the methods that uses the wave spectrum. Prpic-Orsic and Faltinsen (2012) used this time-domain method to calculate speed loss in a seaway. However, the method has not, to the authors' knowledge, been applied in a maneuvering model.

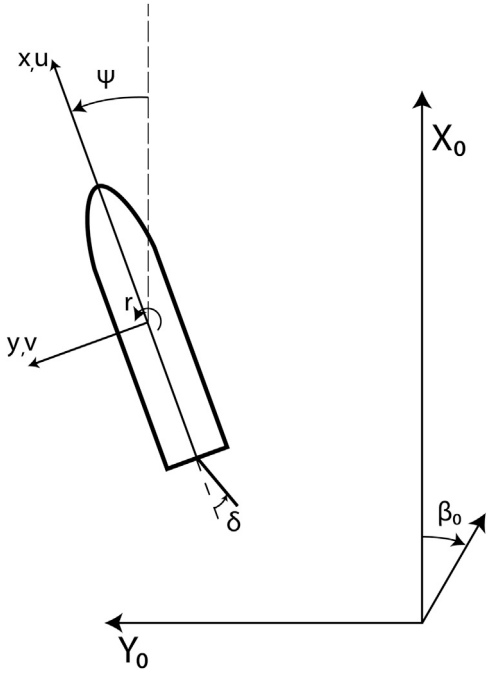

Fig. 1. Body-fixed coordinate system xyz and Earth-fixed coordinate system X_0, Y_0, Z_0. Positive direction of yaw, Ψ, yaw-rate, r, rudder angle, δ, and initial wave heading, β_0 are indicated.

The numerical simulations are compared with experimental results for the Duisburg Test Case (DTC). Turning circles with 35° rudder angle, in regular and irregular waves, for a range of wave conditions, are presented. In irregular waves, the sensitivity to different time realizations, are investigated both experimental and numerical. Furthermore, new dedicated experiments of maneuvers of the DTC hull in irregular waves are presented, and the uncertainty of the experimental results, introduced by variation of the wave height throughout the basin, is investigated.

2. Mathematical model

Two coordinate systems are applied: one right-handed body-fixed coordinate system, xyz, with the z-axis pointing upwards through the center of gravity, with $z = 0$ at calm water level, and one Earth-fixed coordinate system $X_0Y_0Z_0$, which is a right-handed coordinate system with the Z_0-axis pointing upwards. Both coordinate systems are illustrated in Fig. 1.

The mathematical maneuvering model is the same as in Rabliås and Kristiansen (2021), which is a 4-DOF modular model based on Skejic (2008). The equation of motion is provided in Eq. (1).

The hull lifting coefficients, Y_v, Y_p, Y_r, K_v, K_p, K_r, N_v, N_p, and N_r, are calculated by slender body theory, while the zero-frequency added mass terms $X_{\dot{u}}$, $Y_{\dot{v}}$, $Y_{\dot{p}}$, $Y_{\dot{r}}$, $K_{\dot{v}}$, $K_{\dot{p}}$, $K_{\dot{r}}$, $N_{\dot{v}}$, $N_{\dot{p}}$, and $N_{\dot{r}}$ are calculated with the 3D panel code WAMIT. Subscript R, $PROP$, and CF represents rudder loads, propulsion loads, and loads due to viscous flow separation. The transverse viscous loads due to flow separation are calculated with the 2D+t approach presented in Rabliås and Kristiansen (2021). The term C_{TN} is an empirical reduction factor due to viscous effects, in

$$
\begin{bmatrix} M & 0 & 0 & 0 \\ 0 & M & 0 & 0 \\ 0 & 0 & I_{44} & -I_{46} \\ 0 & 0 & -I_{64} & -I_{66} \end{bmatrix} \begin{bmatrix} \dot{u} \\ \dot{v} \\ \dot{p} \\ \dot{r} \end{bmatrix} + \begin{bmatrix} 0 & -Mr & 0 & 0 \\ 0 & 0 & 0 & Mu \\ 0 & 0 & 0 & 0 \\ 0 & 0 & 0 & 0 \end{bmatrix} \begin{bmatrix} u \\ v \\ p \\ r \end{bmatrix} = \begin{bmatrix} X_{\dot{u}} & 0 & 0 & 0 \\ 0 & Y_{\dot{v}} & Y_{\dot{p}} & Y_{\dot{r}} \\ 0 & K_{\dot{v}} & K_{\dot{p}} & K_{\dot{r}} \\ 0 & N_{\dot{v}} & N_{\dot{p}} & N_{\dot{r}} \end{bmatrix} \begin{bmatrix} \dot{u} \\ \dot{v} \\ \dot{p} \\ \dot{r} \end{bmatrix}
$$
$$
+ \begin{bmatrix} 0 & -C_{TN} Y_{\dot{v}} r & -Y_{\dot{p}} r & -Y_{\dot{r}} r \\ 0 & 0 & 0 & X_{\dot{u}} u \\ 0 & 0 & 0 & 0 \\ 0 & -X_{\dot{u}} u & 0 & 0 \end{bmatrix} \begin{bmatrix} u \\ v \\ p \\ r \end{bmatrix} + \begin{bmatrix} 0 & 0 & 0 & 0 \\ 0 & Y_v & Y_p & Y_r \\ 0 & K_v & K_p & K_r \\ 0 & N_v & N_p & N_r \end{bmatrix} \begin{bmatrix} u \\ v \\ p \\ r \end{bmatrix}
$$
$$
- \begin{bmatrix} 0 & 0 & 0 & 0 \\ 0 & 0 & 0 & 0 \\ 0 & 0 & C_{44} & 0 \\ 0 & 0 & 0 & 0 \end{bmatrix} \begin{bmatrix} \int_0^t u dt \\ \int_0^t (v + z_G p + u\psi) dt \\ \phi \\ \psi \end{bmatrix} + \begin{bmatrix} X_R \\ Y_R \\ K_R \\ N_R \end{bmatrix} + \begin{bmatrix} X_{PROP} \\ Y_{PROP} \\ K_{PROP} \\ N_{PROP} \end{bmatrix} + \begin{bmatrix} X_{CF} \\ Y_{CF} \\ K_{CF} \\ N_{CF} \end{bmatrix} + \begin{bmatrix} \overline{R}_X \\ \overline{R}_Y \\ \overline{R}_K \\ \overline{R}_N \end{bmatrix} \tag{1}
$$

the present work $C_{TN} = 0.5$. $\overline{R}$ represents slowly varying second-order loads due to regular or irregular waves. Calm water rudder loads and propulsion loads are calculated with the same conventional methods as in Rabliås and Kristiansen (2021).

The time integration is performed with a fourth-order Runge–Kutta scheme. The time-step is 0.1 in full scale. All time-varying terms in (1), except the slowly varying second order wave loads, are updated at each sub-step of the time integration. The two-time scale assumptions is applied for the wave loads, which means that it is assumed that the slowly varying maneuvering motions have a different time scale than the linear waved induced motions, and only the slowly varying second order wave loads are accounted for. The slowly varying wave loads are decoupled from the rest of the equation system, and they are updated at a different time scale. In regular waves the slowly varying second order wave loads are updated at a predetermined threshold for heading and velocity. Based on a convergence study, where the threshold was systematically varied, the threshold is set to $\Delta\Psi = 2°$ and $\Delta u = 0.2$ m/s (full scale). How the second order wave loads are updated in irregular waves is discussed in Section 2.2.2.

Even though the linear waved induced motions are neglected in the equation of motion (1), it is of high importance to accurately calculate the linear wave induced motions, in order to properly calculate the second order wave loads. In the present work, the linear wave induced motions, in six-degrees of freedom, $\eta_1 - \eta_6$, are solved in the frequency plane with the STF strip theory. The amplitudes and phase angles of the linear wave induced motions are updated at the same threshold as the second order wave loads.

For more information about the numerical model, we refer to Rabliås and Kristiansen (2021). The present paper presents further developments related to effects of waves on the rudder and propeller, and the calculation of second-order wave loads, in regular and irregular waves.

2.1. Wave effects on propulsion and rudder loads

Nakamura and Naito (1975) showed that the wake velocities fluctuate due to waves and ship motions, and the mean of the fluctuations differs from the calm water wake. Furthermore, their experiments indicated that the vessel pitch motion was the dominating cause to the change in wake. The wake velocities affect both the propeller loads and the rudder loads. Hence, it is possible that wave effects on the wake velocities can have a significant effect on the maneuvering behavior.

Faltinsen et al. (1980) proposed a formula that accounts for the increase in mean propeller inflow due to wave induced pitch motion,

$$
V_{mean} = \sqrt{\left(1 - \frac{\Delta\overline{p}}{0.5\rho U^2}\right)} U \tag{2}
$$

where, U is the free stream velocity, ρ is the density of water, and $\Delta\overline{p} \sim -\frac{\rho}{4}\omega_e^2 |\eta_5|^2 x_p^2$ is the pressure gradient due to pitching motion, η_5. ω_e is the encounter frequency and x_p is the x-position of the propeller.

Ueno et al. (2013) presented a method for the fluctuating part of the wake velocity, where the water particle motion and the surge motion of the ship are accounted for.

$$
V_{fluctuating} = (1 - w_p)\left\{U - \omega_e \eta_{1,a} \sin(\omega_e t - \varepsilon_1)\right\} + \alpha\omega\zeta_a \exp(kz_p)\cos\chi\cos(\omega_e t - kx_p\cos\chi) \tag{3}
$$

where w_p is the effective calm water wake fraction, $\eta_{1,a}$ is the amplitude of the surge motion, ε_1 is the phase of the surge motion, ζ_a and k are the wave amplitude and wave number of the incident wave, χ is the wave heading, and z_p is the z-position of the propeller. α is a factor that takes into account that the incident wave amplitude is modified due to the present of the hull,

$$
\alpha = \begin{cases} 0.2\left(\frac{\lambda}{L_{pp}|\cos\chi|}\right) + 0.5, & \text{for } \frac{\lambda}{L_{pp}|\cos\chi|} \leq 2.5 \\ 1, & \text{for } \frac{\lambda}{L_{pp}|\cos\chi|} > 2.5 \end{cases} \tag{4}
$$

where λ is the wavelength and L_{pp} is the length between perpendiculars.

Taskar et al. (2016) combined the method by Faltinsen et al. (1980) and Ueno et al. (2013) to estimate the time varying wake velocity in waves

$$
U_A = \left((1 - w_p)\left\{U - \omega_e \eta_{1,a} \sin(\omega_e t - \varepsilon_1)\right\} + \alpha\omega\zeta_a \exp(kz_p)\cos\chi\cos(\omega_e t - kx_p\cos\chi)\right)\sqrt{\left(1 - \frac{\Delta\overline{p}}{0.5\rho U^2}\right)} \tag{5}
$$

Taskar et al. (2016) compared the predicted wake from (5) with measured wake data from model tests, and a good match between the predicted and measured wake was obtained. In the present work, (5) is used to calculate the inflow to the propeller.

The rudder loads are strongly dependent on the inflow velocity, both the x-component and the y-component. The longitudinal and transverse components of the ambient flow can be written as

$$
\begin{aligned} u_r &= U_A[1 + k_m(\sqrt{1 + C_{th}} - 1)] \\ v_r &= v + x_r r + v_{r,w} \end{aligned} \tag{6}
$$

where U_A is the propeller inflow velocity calculated by Eq. (5), C_{th} is the propeller thrust loading coefficient, k_m accounts for the distance-to-propeller diameter ratio, v is the sway velocity of the ship, r is the yaw rate of the ship, and $v_{r,w}$ is the wave induced velocity in the transverse direction.

When the x-component of the rudder inflow is calculated with Eq. (6), where U_A is calculated by Eq. (5), the effects of waves are implicitly accounted for. To consistently account for the wave modified

inflow velocity, the y-component of the inflow velocity should also be modified due to waves. This has not, to the authors' knowledge, been accounted for earlier. Now we need to establish how to calculate the wave modified inflow velocity in the transverse direction. In (5), the incident wave velocity, and linear wave induced surge- and pitch velocities are accounted for. A first approximation is to account for the same effects as in Eq. (5), namely the incident wave velocity and linear wave induced sway-, roll-, and yaw-velocities. The inflow velocity due to waves can then be written as

$$\begin{aligned} v_{r,w} = & \left(\omega_e \eta_{2,a} \sin(\omega_e t - \varepsilon_2) - z_r \omega_e \eta_{4,a} \sin(\omega_e t - \varepsilon_4)\right. \\ & \left. + x_r \omega_e \eta_{6,a} \sin(\omega_e t - \varepsilon_6)\right) \\ & - \alpha \omega \zeta_a \exp(k z_r) \sin\chi \cos(\omega_e t - k x_r \cos\chi) \end{aligned} \tag{7}$$

where $\eta_{2,a}$, $\eta_{4,a}$, $\eta_{6,a}$, ε_2, ε_4, and ε_6 are the amplitudes and phase angles of the first order wave induced sway, roll, and yaw motion. x_r and z_r are the x- and z-position of the rudder. In the current maneuvering model equation (5)–(7) are used to calculate the inflow velocities to the rudder. The amplitudes and phase angles of the linear wave induced motions, $\eta_{i,a}$ and $\varepsilon_{i,a}$ for $i = 1-6$, are calculated with the STF strip theory in the seakeeping module. The amplitudes and phase angles are updated with the same interval as the second order wave loads.

2.2. Estimation of second-order wave loads

2.2.1. Regular waves

Following a two-time scale assumption, we assume that the maneuvering motions follow a more slowly varying time scale than the linear wave loads. This is in general true for head sea, quartering, and beam side, but may be questionable in following sea. In regular waves, the waves loads are accounted for by the mean second-order drift loads. In Rabliås and Kristiansen (2021) the drift loads were calculated by two methods based on strip theory. For the wave lengths where the ship motions dominates, the drift loads were calculated by the pressure integration method presented by Faltinsen et al. (1980). For the shortest wavelengths where wave reflection dominates, the drift loads were calculated by the asymptotic method in Faltinsen et al. (1980). The linear wave induced ship motions, in six degrees of freedom, are calculated with the STF-strip theory (Salvesen et al., 1970). For some wavelengths both the ship motions and wave reflection will contribute to the drift loads. A modified version of the formula by Fujii (1975) was applied to combine the pressure integration method and asymptotic method, more information can be found in Rabliås and Kristiansen (2021).

In Rabliås and Kristiansen (2021), some discrepancies were observed when the calculated drift loads were compared with experiments, in particular for following waves, and for sway- and yaw-drift. This was suggested to be a main cause for the deviation of the maneuvering simulations compared to experiments. In order to improve the accuracy of the numerical model, the drift loads for regular waves are calculated with a different approach in the present work. The main steps of this approach follows in the next paragraphs.

Yasukawa et al. (2018) measured the drift loads experimentally, on a bulk carrier, for a range of wavelengths, wave headings, and Froude numbers. They observed that while the added resistance was sensitive

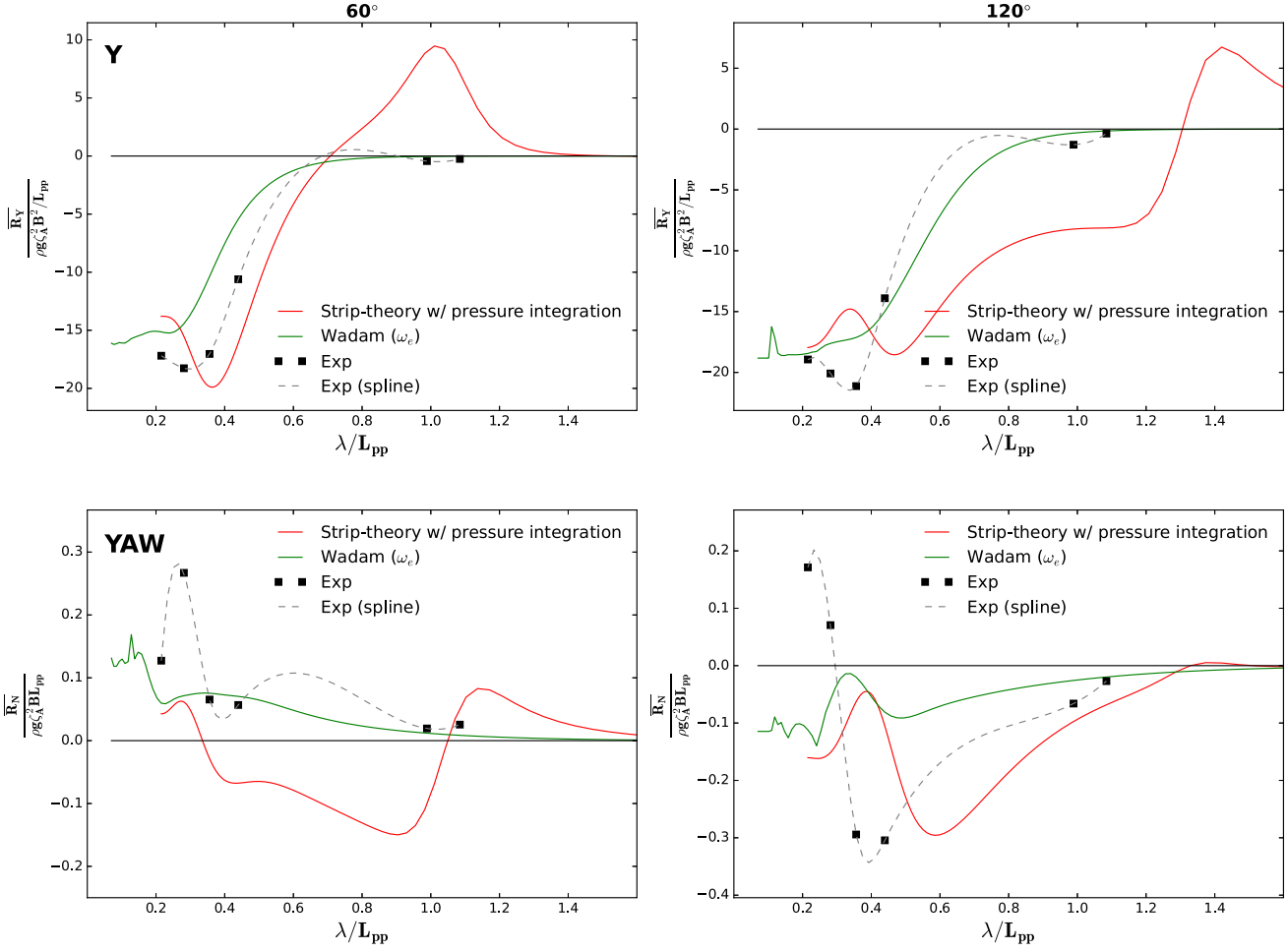

Fig. 2. Mean drift loads for the DTC hull in oblique waves, wave headings 60° (left) and 120° (right) (head sea is 180° and following sea is 0°). Froude number 0.052. Numerical calculations performed with strip-theory with pressure integration and calculations performed with WADAM, are compared with experimental results from Sprenger and Fathi (2015). Upper row: y-drift. Lower row: yaw-drift.

to forward velocity, the forward velocity effect on the lateral drift loads was small. Another observation was that the x- and y-drift were estimated with acceptable accuracy with a strip theory method, while the accuracy of the calculated yaw-moment was not acceptable. Inspired by this, they introduced a modular maneuvering model, where the x-drift was calculated with a strip theory that accounts for forward velocity effects, while the lateral drift was calculated with a 3D panel code without forward velocity effects. A similar approach is implemented in the present work. The x-drift is calculated with the same strip theory as in Rabliås and Kristiansen (2021), while the y- and yaw-drift are calculated with the 3D panel code WADAM, with no forward velocity. The y-drift and yaw-drift loads are pre-calculated for a range of wave frequencies, with 5° spacing in the wave heading. During a simulation the lateral drift loads are interpolated from the pre-calculated table based on the encounter frequency and wave heading. This approach ensures that the forward velocity effects are taken into account for the x-drift, while accuracy of the y- and yaw-drift are improved compared to the results in Rabliås and Kristiansen (2021).

In Fig. 2, the y-drift and yaw-drift, calculated with strip theory with pressure integration and WADAM, for 60° and 120° wave heading and Fn = 0.052, are compared with experiments from Sprenger and Fathi (2015). As an attempt to visualize the trends in the experimental results, a spline representation is included in the figure. We have no information about the experimental values between data points, thus should this spline representation be considered for visualization purposes only. Overall, the drift loads calculated with WADAM, where only the encounter frequency is taken into account, show a better agreement with the experimental results compared to the strip theory with pressure integration. Moreover, sensitivity studies (not presented here) show that turning circles in regular waves compare better with our experiments when the y-drift and yaw-drift are estimated with WADAM.

2.2.2. Irregular waves

In an irregular sea state we can formally write the second-order difference-frequency loads, i.e the slowly varying loads, as

$$F_i^{SV} = \sum_{j=1}^{N}\sum_{k=1}^{N} A_j A_k \left\{ T_{jk}^{ic} \cos\left[(\omega_k - \omega_j)t + (\sigma_k - \sigma_j)\right] + T_{jk}^{is} \sin\left[(\omega_k - \omega_j)t + (\sigma_k - \sigma_j)\right] \right\} \tag{8}$$

where A_i and ω_i are the wave amplitude and circular wave frequency for wave component i in the wave spectrum. $\sigma_i = \varepsilon_i + k_i X_0(t)\cos\chi + k_i Y_0(t)\sin\chi$, where ε_i is a random phase angle, k_i is the wavenumber, $X_0(t)$ and $Y_0(t)$ are the ship position in the global coordinate system, and χ is the wave heading. The coefficients T_{jk}^{ic} and T_{jk}^{is} can be considered as quadratic transfer functions. These coefficients can be challenging and time consuming to compute, especially the off-diagonal terms. Newman (1974) proposed that the coefficients could be approximated as

$$\begin{aligned} T_{jk}^{ic} &= T_{kj}^{ic} = 0.5(T_{jj}^{ic} + T_{kk}^{ic}) \\ T_{jk}^{is} &= T_{kj}^{is} = 0 \end{aligned} \tag{9}$$

Using Eqs. (8) and (9) it is sufficient to calculate the diagonal terms of the quadratic transfer function. Hence, the same methods as for regular waves can be used to calculate the drift loads for each wave component in the spectrum. In the current model, the coefficients T_{jk} are updated at the same threshold as for regular waves, when the heading changes 2° or the forward velocity changes 0.2 m/s,

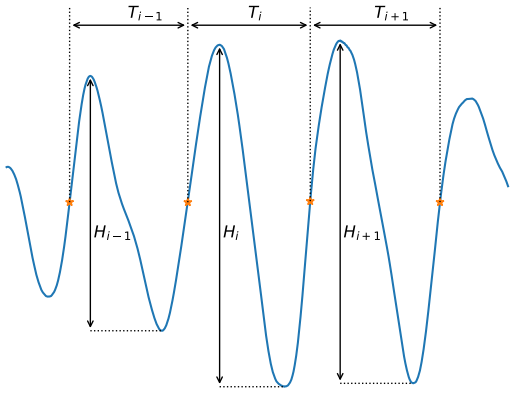

Fig. 3. Example of irregular wave elevation. Zero-upcrossing points are indicated with orange stars. The wave height (H) and wave period (T) for three consecutive waves are indicated with arrows. (For interpretation of the references to color in this figure legend, the reader is referred to the web version of this article.)

while the summation in Eq. (8) is performed every tenth time step to account for the ship motion. Newman (1974) proposed as a further approximation, that Eq. (8) could be simplified by the square of a single sum. This single sum approach was also implemented, which reduced the computational time somewhat. However, the computational time with the double sum was acceptable, and it was considered that we not wanted to approximate the calculations further. Thus the double summation is applied in the current work.

The calculation of the slowly varying drift loads, in irregular waves, with Eq. (8) is based on the wave spectrum, and the random phase angle ε_i ensures that you get a realistic time trace of the loads. An alternative method is a "time-domain" method, first proposed by Hsu and Blenkarn (1972). This method is not based on the wave spectrum, but the time-series of an irregular wave. The irregular time trace of the wave elevation can be considered as a series of regular waves with different wave heights and wavelengths. By locating either zero-upcrossing or zero-downcrossing time instants, a series of individual waves can be obtained. When the zero-crossing (upwards or downwards) time instants are determined, the wave period is taken as the time between two zero-crossing time instants. The wave height is taken as the distance between the maximum wave elevation and the minimum wave elevation between two zero-crossing time instants. An example of an irregular wave elevation, with illustration of how the wave height and wave period are determined is illustrated in Fig. 3. For each wave encounter, the drift loads are estimated as if there was a steady regular wave with wave period and wave height equal to that wave encounter. Prpic-Orsic and Faltinsen (2012) used this method to calculate velocity loss in a seaway. However, this method has not, to the authors' knowledge, been applied in a maneuvering problem earlier. This approach can use measured time-series of the wave elevation directly, or a time-series can be generated from a wave spectrum.

In the original formulation of the "time-domain" method, the wave encounter at the origin of the body-fixed coordinate system, is used in the calculation of the slowly varying drift loads. However, for a container ship, in realistic sea states, a significant number of the waves will be relative short compared to the ship length. This means that there will be several waves along the ship at the same time. As a first approximation to account for this effect, the wave loads are calculated for all waves along the ship, and the weighted sum is used in the maneuvering simulations, where the wave encounter at the origin has most weight. Sensitivity studies (not shown here) indicate that this approach improve the results. However, more research is needed on this topic.

Table 1
Particulars of the presently investigated Duisburg Test Case (DTC) hull.

Particulars		Ship	Model
L_{pp}	[m]	355	5.577
B	[m]	51	0.801
d	[m]	14.5	0.228
Δ	[kg]	173468000	673.27[a]
C_B	[–]	0.661	0.661
x_G[b]	[m]	174.059	2.721[a]
y_G	[m]	0	0
KG	[m]	19.851	0.311[a]
GM	[m]	5.100	0.081[a]
I_{44}	[kgm^2]	7.148E+10	41.51[c]
I_{55}	[kgm^2]	1.322E+12	1294.2[a]
I_{66}	[kgm^2]	1.325E+12	1268.4
L_{bk}	[m]	14.85	0.23[a]

[a]Measured values.
[b]Relative to aft perpendicular.
[c]Estimated from measured natural roll period and numerical added mass.

3. Experimental setup

In January 2020, we performed tests of a 1:63.65 scale model of the Duisburg Test Case in the Ocean basin at SINTEF Ocean in Trondheim. 20/20 Zig-Zag tests and turning circles, with 25° and 35° rudder angle, were tested in calm water, regular and irregular waves, with emphasize on tests in irregular waves. This test campaign was follow-up of the test campaign described in Rabliås and Kristiansen (2019), where the focus was on tests in regular waves.

The test-setup is identical with the setup in Rabliås and Kristiansen (2019), except that rudder loads were measured in the current tests. The model was made at SINTEF Ocean in conjunction with the SHOPERA Project (Sprenger and Fathi, 2015). Before the current test campaign the model was refurbished and repainted. The main particulars of the model are presented in Table 1. Detailed information about the hull, propeller, and rudder can be found in el Moctar et al. (2012).

3.1. Wave documentation

Traditional wave calibration was not performed before the model tests. However, the waves were documented with a significant amount of wave probes distributed in the testing area (without model). The measured wave steepness in general deviates somewhat from the target value. Moreover, the wave amplitude varies slightly throughout the basin. There will also be a deterioration of the wave climate over time due to wave reflection from the beach. Before the model tests, the results from the wave documentation were investigated in detail, such that the maneuvering tests could be performed in the region in the basin where the wave heights had least variation, and that the tests were executed in the most steady time-window.

An overview of the tested wave conditions with representative measures of amplitudes and variation, is presented in Tables 2–3. The regular wave conditions are given in Table 2 and the irregular wave conditions are given in Table 3.

For the regular waves, the time-varying wave height was obtained with the Hilbert-transformation. The irregular waves were generated from a Jonswap wave spectrum with $\gamma = 3.3$. The measured significant wave heights provided in Table 3 are H_{m0}, calculated from the experimental wave spectrum based on the time-series of the wave elevation. The standard deviation over all wave probes in the basin is also presented in Tables 2–3, i.e. how the wave height varies over all wave probes in the basin. The standard deviation is based on the time-averaged wave height for all wave probes in the basin. In Table 2 we can see that the standard deviation is between 8.65% and 9.90% of the mean wave height for the regular waves, while for the irregular waves (Table 3) the standard deviation is between 2.95% and 4.93% of the mean wave height. This indicates that the spatial variation of the wave height is similar for different wave conditions. Moreover, the spatial variation is higher for regular waves than for irregular waves.

In Fig. 4, the variation in wave height for regular wave test 80030 is illustrated. The wave heights in the figure are the time-averaged wave heights after the time-instant when the steady wave environment is reached. Each grid point represents a wave probe. In total 480 wave probes were distributed in the basin, with 2 m spacing. The wavemaker side and beach side of the basin are indicated in the figure, the wavemaker is located at $x = 66.7$ m and the beach starts approximately at $x = 0$ m. In addition, there is a wavemaker on the left side of the basin (not used in the present tests), with a corresponding beach on the right side of the basin. The variation of the wave height is most significant on the sides of the basin, on the right side there are some regions where the wave height is significantly higher than in the rest of the basin, while on the left side of the basin the wave heights are lower than in rest of the basin. Preliminary numerical investigations indicate that the pattern on the right hand side, with increased wave height, is caused by the wave beach at the right hand side, while the pattern on the left hand side is cause by imperfections in the basin wall at the left hand side. In the free running maneuvering tests these regions were, as far as possible, avoided. Relevant testing area of free running

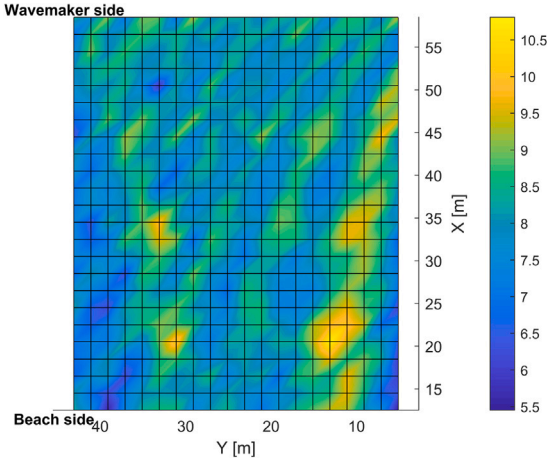

Fig. 4. Example results from wave documentation for regular wave test 80030. Time-averaged wave heights for 480 wave probes are presented, the grid points represent the 480 wave probes. The target wave height is 7.60 m, the mean measured wave height in the basin is 8.08 m, and the standard deviation is 0.8 m. Colorbar in meters (full scale). The wavemaker is located at x = 66.7 m and the beach starts approximately at x = 0 m.

Table 2
Regular wave conditions tested in the present model tests.

Wave ID	λ/L_{pp}	T [s]	H [m]				
			Target	Meas.	Diff.	std	std/H
80010	0.44	9.97	3.88	3.93	+1.29%	0.34 m	8.65%
80020	0.63	11.96	5.58	7.26	+30.11%	0.66 m	9.09%
80030	0.86	13.96	7.6	8.08	+6.32%	0.80 m	9.90%
80040	1.12	15.95	9.93	10.81	+8.86%	1.06 m	9.81%

Table 3
Irregular wave conditions tested in the present model tests.

Wave ID	T_p [s]	H_s [m]				
		Target	Meas.	Diff.	std	std/H_s
85000	9.97	3.12	3.45	+10.58%	0.17 m	4.93%
85010	11.97	3.18	3.56	+11.95%	0.11 m	3.09%
85020	11.97	4.97	5.43	+9.26%	0.16 m	2.95%
85030	13.96	4.33	4.71	+8.78%	0.16 m	3.40%
85040	11.97	8.0	8.57	+7.13%	0.28 m	3.28%

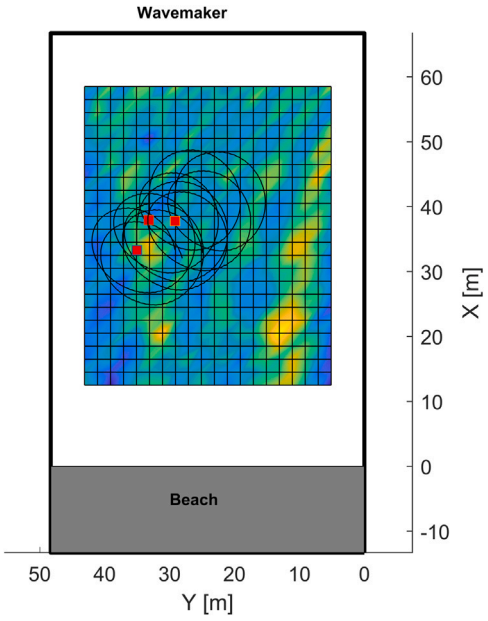

Fig. 5. Trajectory of three experimental repetitions of turning circles with 35° rudder angle in initial head sea. The starting positions of the tests are indicated with red squares. The outer sides of the basin, the beach area, and the position of the wavemaker are indicated. In the area of the basin where results from the wave documentation are available, the time-averaged wave heights are illustrated with a colormap. The colormap is the same as presented in Fig. 4 (WAVE ID 80030).

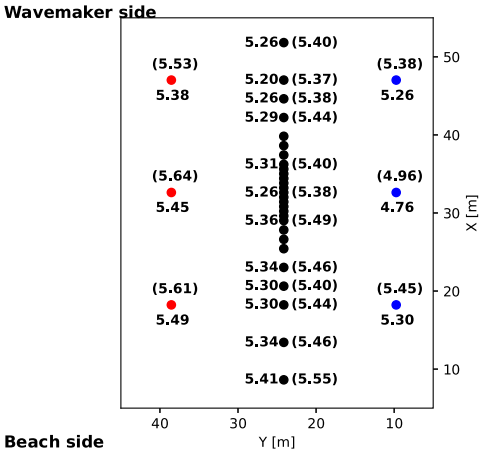

Fig. 6. Overview of wave probe positions of the 35 wave probes used in the documentation of irregular waves. Wave probes are indicated by circular dots. Results, for selected wave probes, for wave 85020 are indicated. The numbers without parenthesis are $H_{1/3}$ calculated from zero-crossing analysis of measured time series, while the numbers in parenthesis are $H_s = H_{m0}$ calculated from spectral analysis of the measured time series. The target significant wave height for this sea state was H_s = 4.97 m. The measured values are significant higher than the target value. The wavemaker is located at x = 66.7 m and the beach starts approximately at x = 0 m.

maneuvering tests is exemplified in Fig. 5, where three experimental repetitions of a turning circle with 35° rudder angle, are indicated in the same figure as a colormap of the time-averaged wave heights. The starting positions of the maneuver are indicated with red squares. The target wave height and wave period are H = 8.08 m and T = 13.96 s, and the incident wave direction is head sea. The outer sides of the basin, the beach area, and the position of the wavemaker are indicated in the figure. The colormap of the wave heights is the same as in Fig. 4. The wave height in the basin varies also with time, hence Figs. 4–5 are only for illustration purposes.

For the documentation of the irregular waves, the wave probes were arranged slightly different compared to the documentation of regular waves. Most of the wave probes were located along the center line of the basin, with some extra wave probes closer to the sides, 35 wave probes in total. The arrangement is illustrated in Fig. 6. Some results from the documentation of wave 85020 are also presented in the figure, to exemplify the results. The significant wave heights are indicated next to the wave probes. The numbers without parenthesis represents $H_{1/3}$, calculated from a zero-crossing analysis of the measured time series, while the numbers in parenthesizes represents $H_s = H_{m0}$, calculated from the wave spectrum based on the measured time series. The significant wave heights calculated from the measured wave spectrum are slightly higher than the significant wave heights calculated from a zero-crossing analysis. However, the difference between the significant wave heights calculated from the wave spectrum and time-series are relatively small, and within the range we could expect. The results in Fig. 6 indicate that the variation of the significant wave height is relatively small along the center line of the basin, below 4%, while there are more variation of the significant wave height for the wave probes along the sides of the basin. This is in accordance with the observations in Fig. 4.

The irregular waves were documented for 22 min (model scale). Due to short waves traveling slowly, it take some time to obtain the wanted sea state in the basin. To ensure that we had a “steady” sea state, no model tests were initiated the first five minutes after the wavemaker started. Moreover, the five first minutes of the measurement are disregarded when the time-series of the wave documentation are post-processed. This means that the measured wave spectra and significant wave heights are based on 17 min of wave documentation, which corresponds to 2 h and 15 min in full scale. After 22 min the wavemaker repeats the signal.

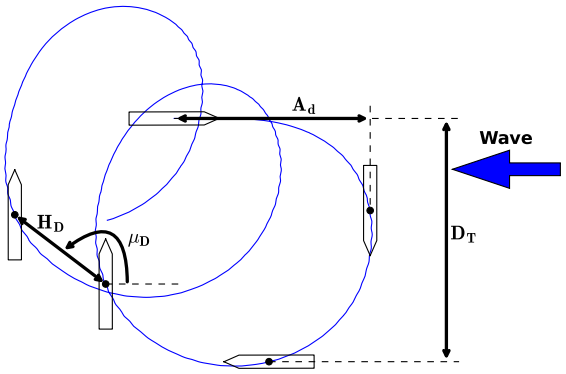

Fig. 7. Definitions of Advance (A_d), tactical diameter (D_T), drifting distance (H_D), and drifting angle (μ_D) during a turning circle in waves.

4. Results

In this section, numerical and experimental results are presented for turning circles with 35° rudder angle, with the DTC hull. Results are presented for calm water and a range of different regular and irregular wave conditions. All simulations are performed in model scale. For presentation purposes, the results presented in this section, are scaled to full scale by Froude scaling. In order to evaluate the results, and observe trends, for a range of conditions, some global responses are chosen to present the results. These are: the tactical diameter (D_T), advance (A_d), drifting distance (H_D), and the drifting angle (μ_D), their definitions are illustrated in Fig. 7.

First, results for calm water are presented to verify the calm water maneuvering model. The trajectory and roll motion of the DTC hull during a turning circle with 35° rudder angle towards starboard, in calm water, with initial velocity corresponding to a Froude number equal to 0.14, are presented in Figs. 8–9. The trajectory is in good agreement with experimental results. However, the steady roll angle is underestimated in the numerical simulations compared to the experiments. The steady roll angle estimated with the numerical model is approximately 40% lower than the experimental results, which indicates that all physical effects in the roll equation are not represented adequately.

Since the calm water maneuvering in the present work is based on the maneuvering model in Rabliås and Kristiansen (2021), results for calm water will not be discussed further, and we refer to Rabliås and Kristiansen (2021) for more comprehensive results and discussions.

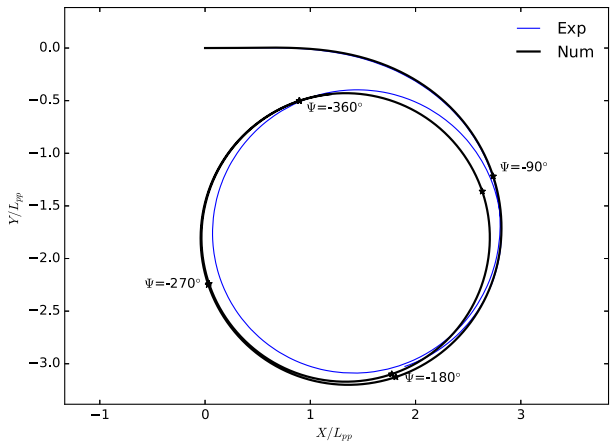

Fig. 8. Trajectory of a turning circle of the DTC hull with 35° rudder angle in calm water. The initial velocity corresponds to a Froude number, Fn = 0.14. Time instants for heading $\Psi = -90°, -180°, -270°$, and $-360°$ are indicated for the numerical results.

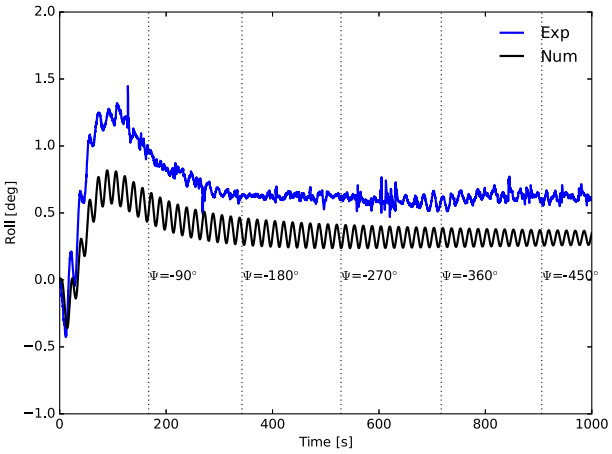

Fig. 9. Roll motion of the DTC hull during a turning circle with 35° rudder angle in calm water. The initial velocity corresponds to a Froude number, Fn = 0.14. Time instants for heading $\Psi = -90°, -180°, -270°$, and $-360°$ are indicated for the numerical results.

4.1. Regular waves

4.1.1. Wave effects on propulsion and rudder loads

The sensitivity to the variation of the inflow velocity to rudder and propeller due to regular waves, for turning circles with 35° rudder angle, is presented in this section. Simulations where the inflow velocity is estimated by Eqs. (5) and (7) are compared to simulations where only the effective calm water wake fraction w_p is taken into account.

The vessel trajectory and propeller thrust obtained by the simulations and experiments in regular waves, with wavelength $\lambda/L_{pp} = 0.63$, are presented in Fig. 10. Overall, the predicted propeller thrust from simulations is in good accordance with experiments. However, the propeller thrust from numerical simulations are slightly lower than the measured thrust. For the simulations where the wave dependent wake is applied, the oscillations have similar amplitude as the experiments. The high frequency oscillations are most prominent, but some low frequency behavior due to waves are also present.

In the beginning of the maneuver, the two methods predict almost identical trajectory. The difference grows with time, and it is most evident around heading $\Psi = -540°$. The difference between the two methods is smaller than the difference between simulations and the experiments. However, the effect of waves on the propeller and rudder inflow is not insignificant.

The tactical diameter, advance, drifting distance, and drifting angle for a range of wavelengths are presented in Fig. 11. For wavelengths $\lambda/L_{pp} = 0.438$ and 0.86, 95% confidence intervals, based on repetition tests, are indicated with error bars for the experimental results. We note that while the stochastic uncertainty is relative low for advance and tactical diameter, the stochastic uncertainty is significantly higher for drifting distance and drifting angle, especially for wavelength $\lambda/L_{pp} = 0.86$. However, for wavelength $\lambda/L_{pp} = 0.86$, the confidence interval is based on three repetitions only. For wavelength $\lambda/L_{pp} = 0.63$ and shorter, the simulations with calm water wake fraction and wave modified inflow velocity predict very similar results. For wavelengths $\lambda/L_{pp} = 0.86$ and 1.12, the two models predict different results, which suggest that the effect of waves on the propeller and rudder inflow is most important for long waves.

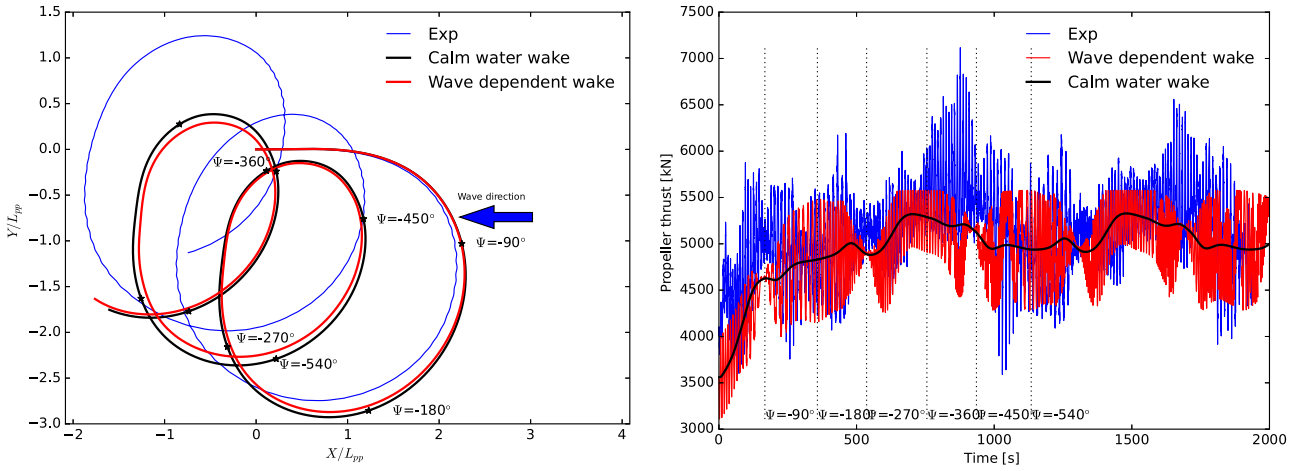

Fig. 10. Results of a turning circle of the DTC hull with 35° rudder angle in regular waves with wavelength λ/L_{pp} = 0.63, wave steepness H/λ = 1/40, head sea (β_0 = 180°) incident wave direction, and 13.92 knots approach velocity (Fn = 0.12). Simulations with calm water wake, and where the inflow to the propeller and rudder is modified due to waves, are compared with experimental results. Incident wave direction is indicated with an arrow. Time instants for heading Ψ = −90°, −180°, −270°, −360°−450°, and −540° are indicated for the simulation where calm water wake is applied. Left: Trajectory. Right: Propeller thrust.

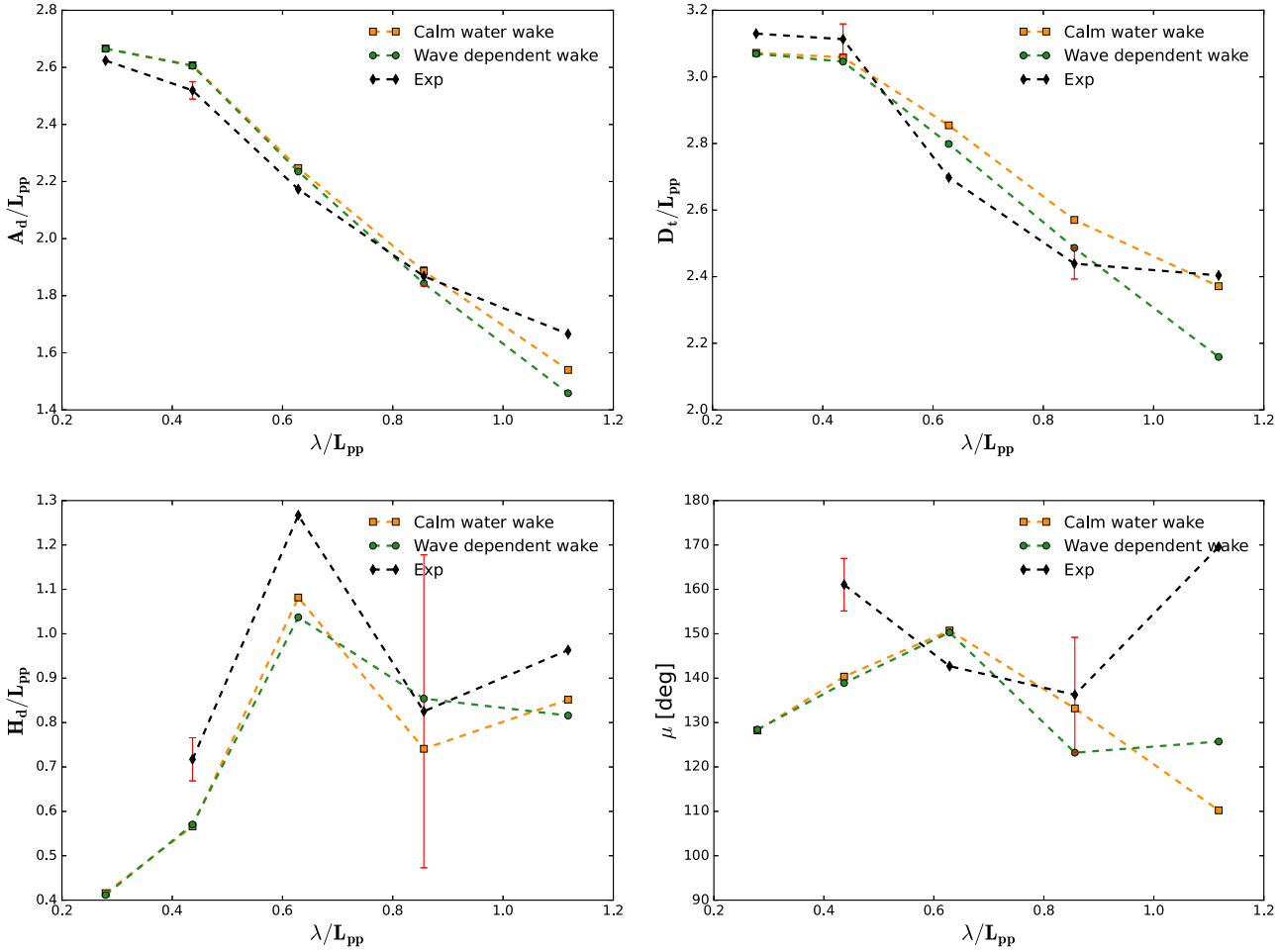

Fig. 11. Experimental and numerical results of a turning circle of the DTC hull with 35° rudder angle in regular waves, for a range of wavelengths in initial head sea. Simulations where calm water wake fraction are applied is compared to simulations where inflow to the propeller and rudder is modified due to regular waves. 95% confidence intervals, based on repetition tests, are indicated with error bars for the experimental results with wavelength λ/L_{pp} = 0.438 (five repetitions) and 0.86 (three repetitions). Upper row: Advance and tactical diameter. Lower row: Drifting distance and Drifting angle.

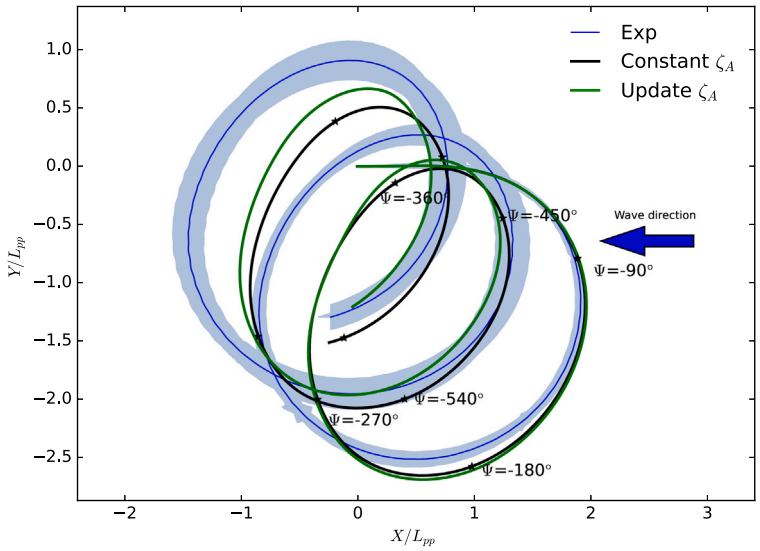

Fig. 12. Trajectory of a turning circle of the DTC hull with 35° rudder angle in regular waves with wavelength λ/L_{pp} = 0.86, head sea (β_0 = 180°) approach angle, and 11.14 knots approach velocity (Fn = 0.1). Simulations with constant wave height, H = 8.02, and simulations where the wave height is updated for each time instant where the drift loads are calculated, are compared to experimental results. For the experimental results, the mean path, based on repetition tests, is given, and in addition the shaded area represents the standard deviation due to three repetition tests. Incident wave direction is indicated with an arrow. Time instants for heading Ψ = −90°, −180°, −270°, −360°−450°, and −540° are indicated for the simulation where constant wave height is applied.

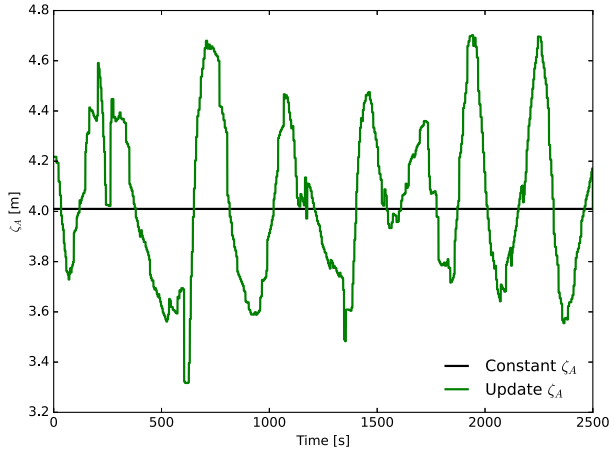

Fig. 13. Example of variation of wave amplitudes during a turning circle with 35° rudder angle in regular waves with wavelength λ/L_{pp} = 0.86. The black line represents the mean wave amplitude measured in the basin (see Fig. 4). The green line represents the time- and space-varying wave amplitudes measured in the basin. The two vessel paths using mean and varying wave amplitudes are presented in Fig. 12. (For interpretation of the references to color in this figure legend, the reader is referred to the web version of this article.)

4.1.2. Sensitivity to variation of wave height

The second-order wave loads is in general the dominating contribution from the wave environment during maneuvering in waves. Since the second-order loads are proportional to the wave amplitude squared, in general a moderate uncertainty in the wave amplitude can introduce a significant uncertainty in the results. In a wave basin, the wave amplitude varies slightly throughout the basin, as documented in Section 3.1. This can for example be due to the accuracy of the wave maker, uneven bottom, equipment mounted in the basin or at the side walls, and the shape of the wave beach. When experiments are compared with numerical simulations, where the wave height typically is assumed to be constant, the variation in wave height throughout the basin can introduce an uncertainty to the results. This issue is, to some degree, present in all wave basins, and it is important to have an idea of the magnitude of the uncertainty this introduces. Furthermore, if one have information of how the wave climate varies throughout the basin, this uncertainty can be minimized by performing the experiments in the most steady region of the basin.

In this section, simulations in regular waves with constant wave amplitude are compared to simulations in a ”virtual wave basin”. In the ”virtual basin” the wave amplitude is updated, from time-series of the wave documentation described in Section 3.1. For each time step where the second-order wave loads are calculated, the wave amplitude is obtained from measurements of the wave elevation at the position of the ship. Before a simulation, a run from the free-running experiments is used as a reference, such that the initial position in the basin and the time instant when the maneuver begins, can be determined. This ensures that the time-series of the wave elevation in the numerical simulations is as similar as possible to the experiments.

The trajectory of simulations of turning circles with 35° rudder angle in regular waves with wavelength λ/L_{pp} = 0.86, with constant wave amplitude and with space- and time-varying wave amplitude are presented in Fig. 12. The wave amplitudes for these two simulations are presented in Fig. 13. At some time instants the measured local wave amplitude deviates significantly, up to 17.3%, from the mean value in the basin, and it oscillates around the mean value. In the beginning of the maneuver these two simulations follows each other closely, while the difference grows from heading Ψ = −360°. This trend is recognized in Fig. 14, where the tactical diameter, advance, drifting distance, and drifting angle are presented for a range of wavelengths. For tactical diameter and advance, the difference is below 3.5%, for all conditions, when the wave amplitude is updated compared to using a constant wave height. There are more prominent differences for the drifting distance and drifting angle, especially for the longest waves. These results illustrates that variation of the wave height throughout the basin can introduce a significant uncertainty in some responses. However, the deviation is in general less than we expected, and several responses are nearly unaffected. This has practical consequences in light of existing published maneuver experiments.

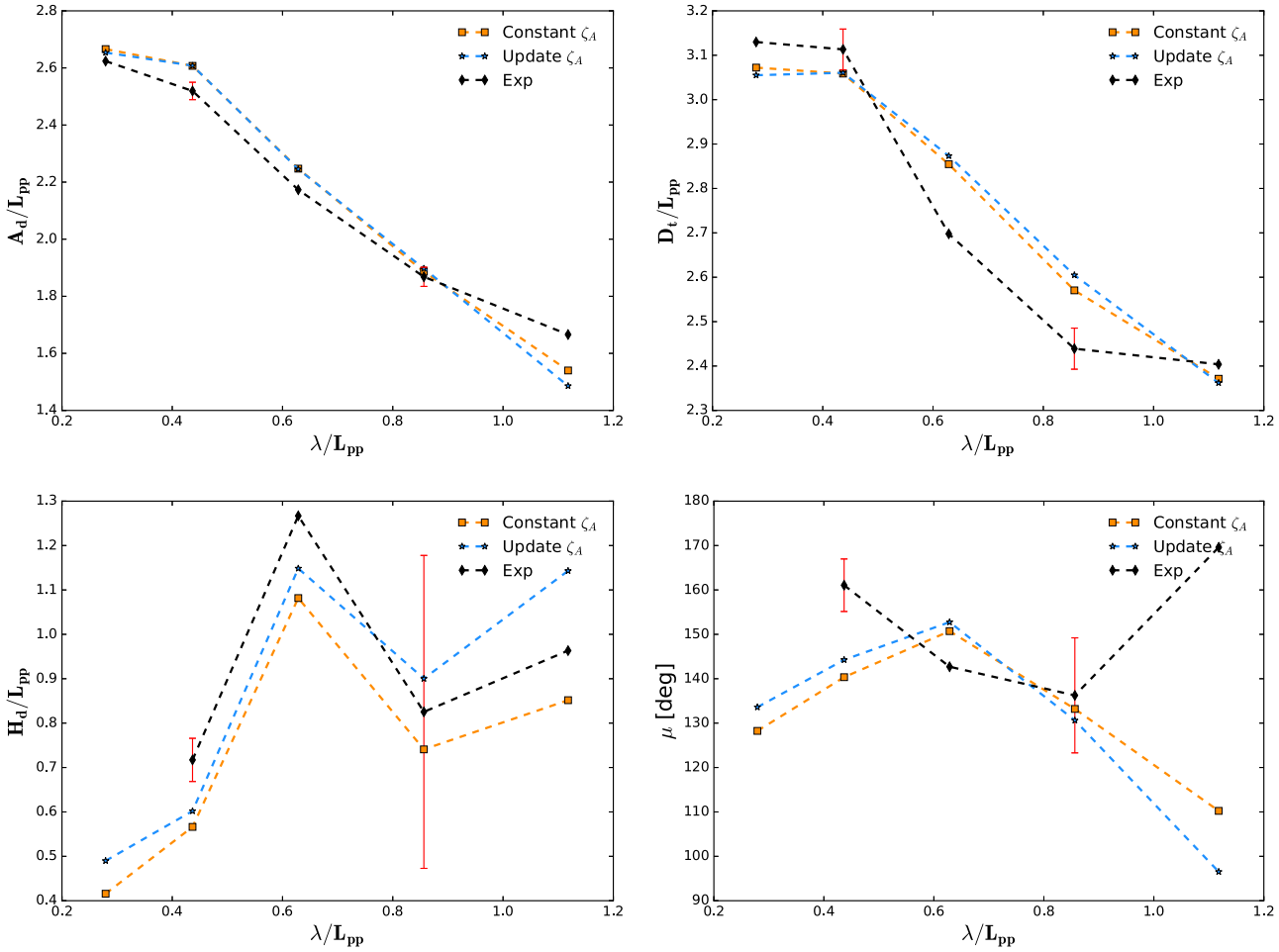

Fig. 14. Experimental and numerical results of a turning circle of the DTC hull with 35° rudder angle in regular waves, for a range of wavelengths in initial head sea. Simulations with constant and varying wave amplitude are compared with experimental results. 95% confidence intervals, based on repetition tests, are indicated with error bars for the experimental results with wavelength λ/L_{pp} = 0.438 (five repetitions) and 0.86 (three repetitions). Upper row: Advance and Tactical diameter. Lower row: Drifting distance and Drifting angle.

4.2. Irregular waves

In this section experimental and numerical results of turning circles with 35° rudder angle, with the DTC hull, are presented for a range of irregular sea states. Results of numerical simulations where the drift loads are calculated with the two methods described in Section 2.2.2, the time-domain method and the Newman approximation with double sum, are presented.

In Section 4.1, it was shown that the wave modified inflow velocity to rudder and propeller, and the variation of wave height, could influence the maneuvering behavior. These effects are therefore included in the simulations in irregular waves. For the time-domain method, measured time-series of the wave elevation are applied. A reference run of the free running experiments is used to synchronize the starting time and starting position of the maneuver. This ensures that the wave elevation in the numerical simulations are as close to experiments as possible. The numerical results are compared with this reference run. For the simulations where the slowly varying loads are calculated with the Newman approximation, wave spectra based on the measured wave elevation are applied. Wave spectra are calculated for all wave probes along the center line of the basin (see Fig. 6), the mean of these wave spectra is then applied in the calculations. To calculate the slowly varying loads, the wave spectrum is divided into 50 components.

The trajectory, surge velocity, sway velocity, and the yaw-rate, for a turning circle with 35° rudder angle, in an irregular sea state with T_p = 11.97 s and H_s = 4.96 m (WAVE ID 85020), initial head sea (β_0 = 180°) approach angle, are presented in Figs. 15–18. The initial velocity is 15.10 knots, which corresponds to a Froude number Fn = 0.13.

Considering the trajectory in Fig. 15, the simulation where the time-domain method is applied for the drift-loads follows the experimental results more closely in the initial phase, compared to the simulation where the slowly varying loads with the Newman approximation is applied. Both methods under-estimate the drift. However, the time-domain method predicts the drift distance best. In Fig. 16 we can see that both methods predict the velocity drop in the initial phase correctly, while there is more deviation later in the maneuver. This is so in particular in following sea, where the experiments shows an increase in the surge velocity. This indicates that the added resistance in following waves is not predicted correctly, which is in accordance with the observations for regular waves in Rabliås and Kristiansen (2021). Since the same method as in Rabliås and Kristiansen (2021) is used to calculate the added resistance, some discrepancies for the added resistance in following sea were expected also in irregular waves.

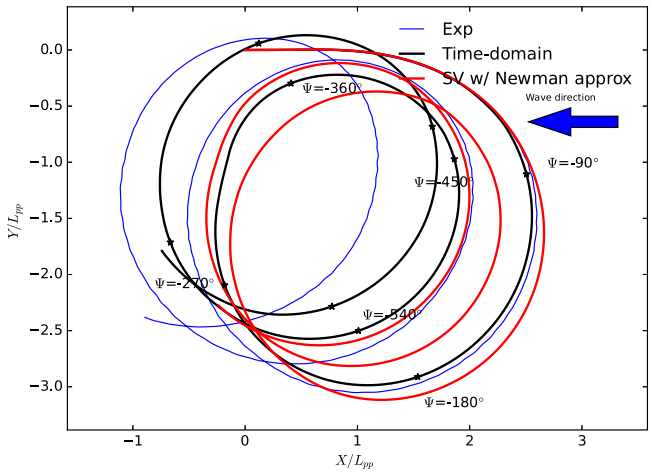

Fig. 15. Trajectory of a turning circle of the DTC hull with 35° rudder angle in an irregular sea state with T_p = 11.97 s and H_s = 4.96 m (WAVE ID 85020), in initial head sea (β_0 = 180°) approach angle, and 15.10 knots approach velocity (Fn = 0.13). Simulations where the drift loads are calculated with the time-domain method, and the Newman approximation are compared with experimental results. Incident wave direction is indicated with an arrow. Time instants for heading Ψ = −90°, −180°, −270°, −360°, −450°, and −540° are indicated for the simulation where the time-domain method is applied.

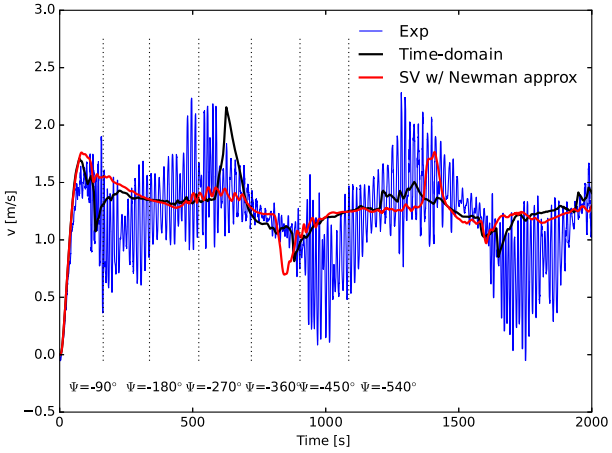

Fig. 17. Sway velocity during a turning circle of the DTC hull with 35° rudder angle in an irregular sea state with T_p = 11.97 s and H_s = 4.96 m (WAVE ID 85020), in initial head sea (β_0 = 180°) approach angle, and 15.10 knots approach velocity (Fn = 0.13). Simulations where the drift loads are calculated with the time-domain method, and the Newman approximation are compared with experimental results. Time instants for heading Ψ = −90°, −180°, −270°, −360°, −450°, and −540° are indicated for the simulation where the time-domain method is applied.

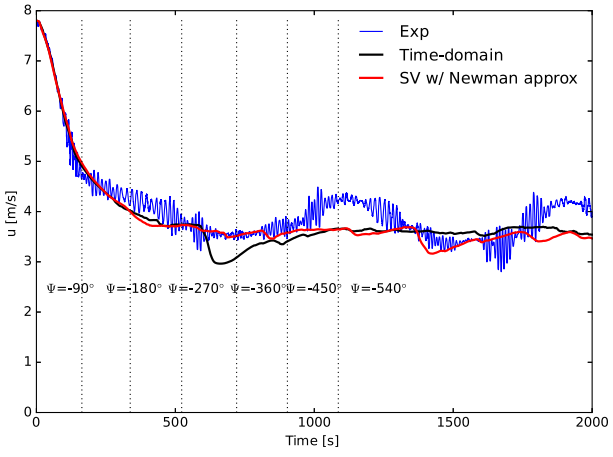

Fig. 16. Surge velocity during a turning circle of the DTC hull with 35° rudder angle in an irregular sea state with T_p = 11.97 s and H_s = 4.96 m (WAVE ID 85020), in initial head sea (β_0 = 180°) approach angle, and 15.10 knots approach velocity (Fn = 0.13). Simulations where the drift loads are calculated with the time-domain method, and the Newman approximation are compared with experimental results. Time instants for heading Ψ = −90°, −180°, −270°, −360°, −450°, and −540° are indicated for the simulation where the time-domain method is applied.

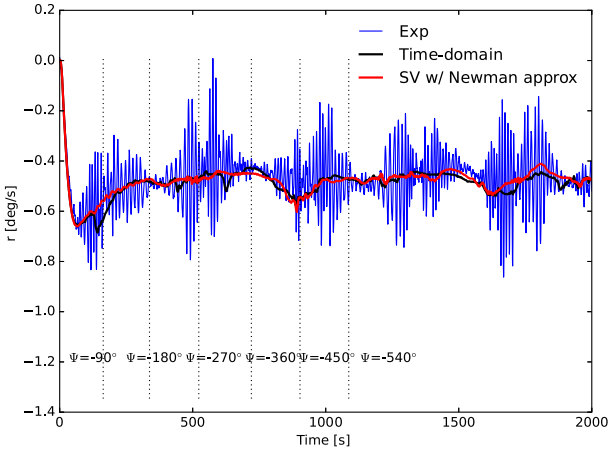

Fig. 18. Yaw rate during a turning circle of the DTC hull with 35° rudder angle in an irregular sea state with T_p = 11.97 s and H_s = 4.96 m (WAVE ID 85020), in initial head sea (β_0 = 180°) approach angle, and 15.10 knots approach velocity (Fn = 0.13). Simulations where the drift loads are calculated with the time-domain method, and the Newman approximation are compared with experimental results. Time instants for heading Ψ = −90°, −180°, −270°, −360°, −450°, and −540° are indicated for the simulation where the time-domain method is applied.

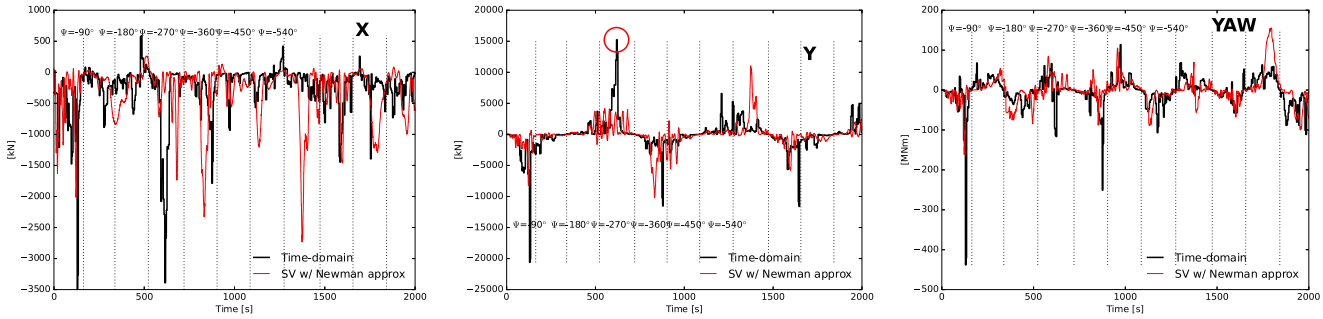

Fig. 19. Slowly varying second order wave loads during a turning circle of the DTC hull with 35° rudder angle in an irregular sea state with T_p = 11.97 s and H_s = 4.96 m (WAVE ID 85020), in initial head sea (β_0 = 180°) approach angle, and 15.10 knots approach velocity (Fn = 0.13). Left: x-drift. Middle: y-drift. Right: yaw-drift.

The sway velocity and yaw-rate, in Figs. 17 and 18 are in reasonably good agreement with experiments for both the time-domain method and the method using the Newman approximation. Due to the two-time scale assumption only the slowly varying surge velocity, sway velocity, and yaw rate are included in Figs. 16–18, for the numerical results. For the experimental results the first order wave induced velocities are also included, which explains the wave-frequency oscillations. The reduction in the sway velocity around heading $\Psi = -90°$ is better represented with the time-domain method. However, there are some local peaks in both the sway velocity and the yaw rate, e.g. at heading $\Psi = -315°$, in the time-domain method. The slowly varying second order wave loads during the maneuver are presented in Fig. 19. The second order wave loads calculated with the difference frequency method and the time-domain method share the same qualitatively behavior, but the time-domain method has narrower and more distinct peaks. For example, the peak in the sway velocity at heading $\Psi = -315°$ coincides with a peak in the y-drift, for the time-domain method (indicated with a red circle in Fig. 19). These peaks are not physical, and represent a weakness of the method. One explanation of these peaks is the nature of the method, where the drift loads are calculated for every wave encounter, and memory effects are therefore not accounted for. This means that extreme waves will influence the drift loads to a larger extent than that in reality. This is confirmed in Fig. 20, where the wave amplitudes of individual wave encounters that are used in the calculation of second order wave loads, with the time-domain method, during the maneuver, are presented. The peak in the y-drift coincides with the wave encounter with the highest wave amplitude during the maneuver (marked with a red circle in Fig. 20). Moreover, if the numerical calculation, for the mean wave drift load, for this specific wave period and wave heading is inaccurate, this effect will be magnified. Since the method using the Newman approximation, includes contribution from all components of the wave spectrum, the behavior is more smoothed and these peaks are less prominent. We acknowledge that more research is needed to eliminate these peaks. However, the velocities returns quickly back to the correct magnitude, and it seems like the overall results are not affected by this behavior.

In Fig. 21 the advance, tactical diameter, drifting distance, and drifting angle, are presented for the five considered irregular sea states. The corresponding H_s and T_p can be found in Table 3. Both the time-domain method and the method using the Newman approximation follow the same trends as the experiments. However, the time-domain method is in general somewhat closer to the experimental results.

Overall, the time-domain method and the method using the Newman approximation show similar accuracy. The main motivation to use the time-domain method is therefore to reduce the computational effort compared to using the Newman approximation. In the current work, the time-domain method is 10–100 faster than the method using the Newman approximation. In the Newman approximation, the wave spectrum was divided into 50 components. If the wave spectrum is divided into more components, the computational time will increase further. Another difference is that the time-domain method accounts

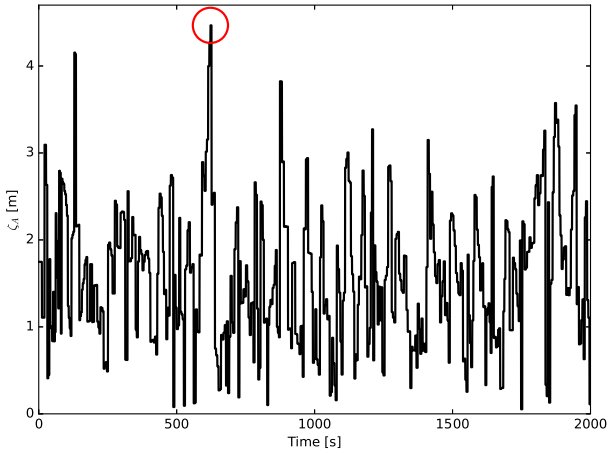

Fig. 20. Wave amplitudes of individual wave encounters that are used in the calculation of second order wave loads, with the time-domain method, during a turning circle with 35° rudder angle.

for the actual wave elevation, which means that extreme waves affects the drift loads directly. This can be an advantage when you compare numerical simulations with experiments, since the exact same time-series of the waves can be applied. Also in ship simulators this can be an advantage, that the loads on the ship correspond to the visualization of the waves. However, a weakness of the time-domain method is that numerical inaccuracies for certain wave frequencies and headings together with high encounter wave heights, can cause nonphysical peaks in the velocities, as exemplified above.

Considering the results in Figs. 15–21, it is important to remember that the experimental results are for a specific test, corresponding to the tests that are used as reference runs for the time-domain method. Since the numerical method using the Newman approximation uses random phase angles, ϵ, in reality the wave-elevation is not identical to the ones used in the time-domain method and in the experimental results. Moreover, it is expected that different time-realizations of the same wave spectrum will affect the results. This is investigated in the following paragraphs.

The effect of different time-realizations of the same wave spectrum, i.e. different time-series of the wave elevation, is presented in Fig. 22. Advance, tactical diameter, drifting distance, and drifting angle, from experimental turning circles of the DTC hull with 35° rudder angle, are presented for the same irregular sea states as considered so far. For each sea state, the maneuver is repeated in different time-windows in the wave spectrum, i.e. the time signal of the wave elevation is different. The maneuver is repeated 5 to 10 time windows for each sea state. The mean values, based on the actual performed number of repetitions, are presented. In addition, 95% confidence intervals are indicated with error bars. The 95% confidence intervals are calculated

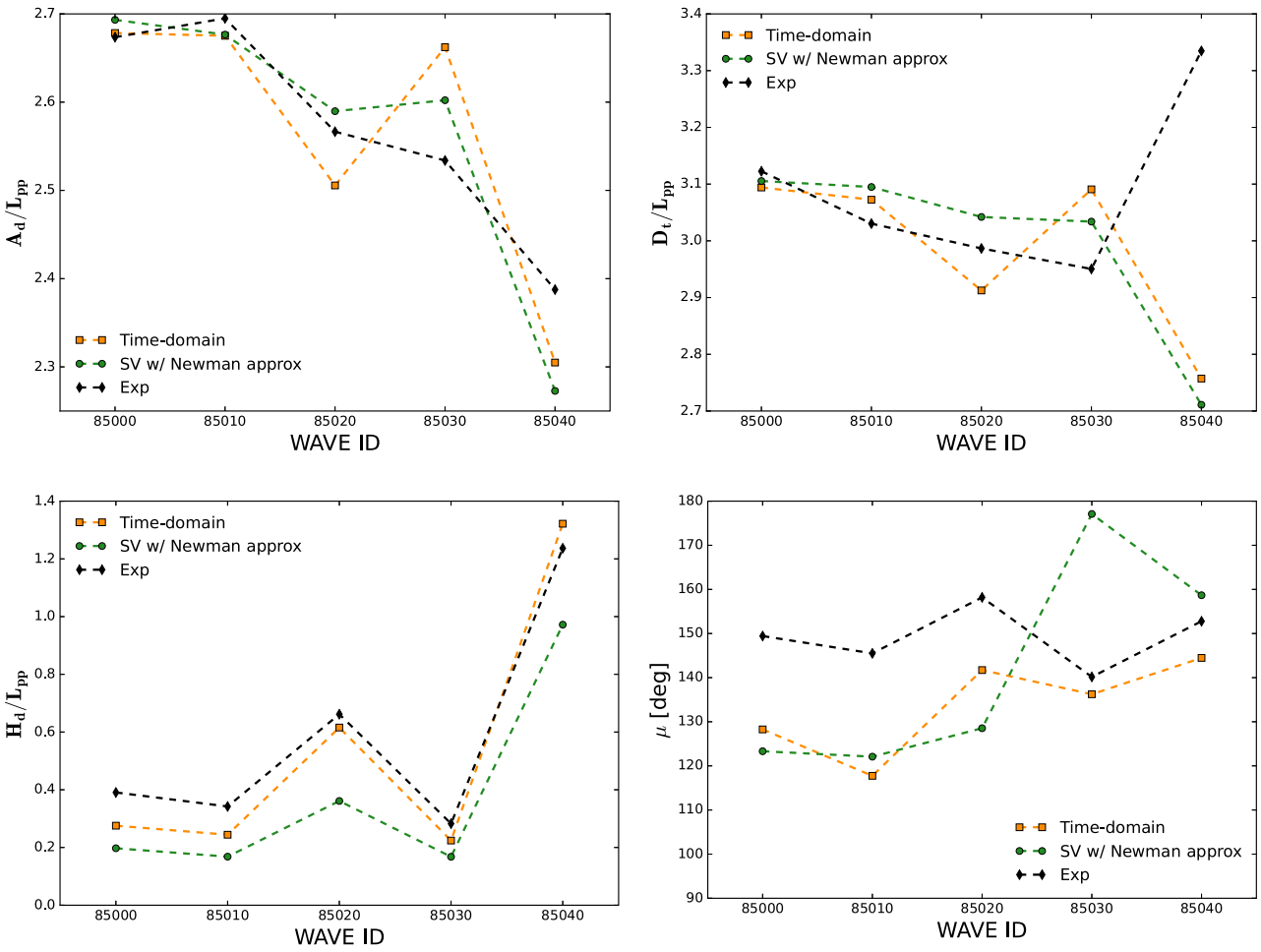

Fig. 21. Experimental and numerical results of turning circles of the DTC hull with 35° rudder angle in five different irregular sea states, in initial head sea. Upper row: Advance and tactical diameter. Lower row: Drifting distance and Drifting angle.

according to ITTC (2014). The confidence intervals are sensitive to the numbers of repetitions, N, especially when relative few repetitions are available. To illustrate the sensitivity to N, the confidence intervals are presented with different values of N. As expected, the confidence intervals decrease when N increases.

If we disregard sea state 85040, which represents adverse weather, the confidence intervals for advance and tactical diameter are below 2.6% of the mean values, while for sea state 85040 the confidence intervals are 4.9% and 9.2% for advance and tactical diameter. The confidence intervals for drifting angle are below 10% of the mean values for all sea states. Considering the drifting distance, the relatively uncertainty is significantly higher than for the other responses. When the confidence intervals are calculated with $N = 5$, the highest relative uncertainty is observed for sea state 85030, where the confidence interval is 42.9% of the mean value. However, if the confidence interval is calculated with $N = 10$, the relative uncertainty is 18.2% for this sea state. The high variation in this response indicate high sensitivity to one, or more probably, a range of physical effects. This is consistent with the results for regular waves, where the stochastic uncertainty was significant for some responses. This could also be one of the reasons to the discrepancies between the numerical results and experiments.

For some conditions, repetition tests in the same time-window were performed (not presented here). The maneuvers were initiated at the same position (within one meter) and the same time instant (within 1 s). The results from these repetition tests indicate that the stochastic uncertainty, for the same realization, is less than the difference between different realizations in the same wave spectrum.

The sea state with $H_s = 4.33$ m and $T_p = 13.96$ s (WAVE ID 85030) is further investigated in Fig. 23, where the cumulative mean and 95% confidence intervals are presented as function of N. Experimental values are presented for 10 realizations, while numerical simulations are presented for up to 30 realizations of the same wave spectrum. In the numerical simulations, the wave elevation is obtained from the experimental wave spectrum, with deterministic amplitudes and random phase angles. The width of the 95% confidence intervals based on numerical simulations and experiments are similar. However, the experiments were only performed for 10 different time-windows, which means that the width of the experimental confidence intervals are not converged.

Based on the numerical results in Fig. 23, the 95% confidence intervals of the advance and tactical diameter are below 1.4% of the mean value when the number of realizations $N \geq 5$, both when the drift loads are calculated with the time-domain method and the Newman approximation. The 95% confidence intervals in the experiments are also low, but about twice as high, 2.51% and 1.58% of the mean values for advance and tactical diameter after 5 realizations, while after 10 realizations the confidence intervals are 1.51% and 0.75% of the mean values.

The drifting distance and drifting angle are more sensitive to number of realizations of the same spectrum. After 10 experimental realizations, the 95% confidence interval for the drifting distance is 25.4% of the mean value. After 10 numerical realizations with the time-domain method and the Newman approximation, the confidence intervals are 20.6% and 23.7% of the mean value. 29 numerical realizations with the Newman approximation are needed before the 95% confidence interval

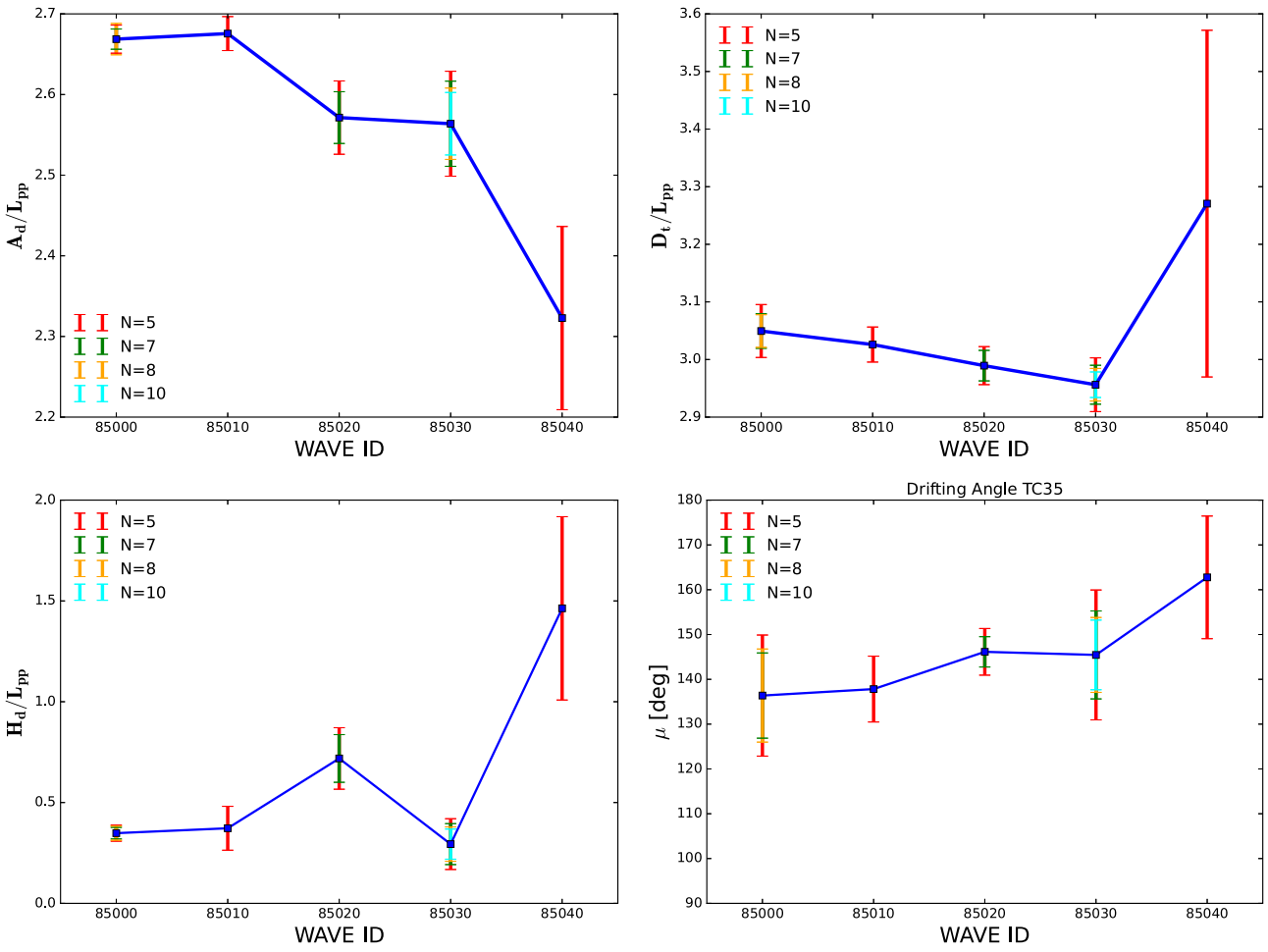

Fig. 22. Experimental results of turning circles of the DTC hull with 35° rudder angle in five different irregular sea states. The sea states corresponding to the Wave IDs in the figure are given in Table 3. The experiments are performed for different time series in each sea state. The mean value and 95% confidence intervals are presented. The 95% confidence intervals are presented for different values of repetitions, N. Upper row: Advance and tactical diameter. Lower row: Drifting distance and Drifting angle.

for the drifting distance is below 10% of the mean value. With the time-domain method, the 95% confidence intervals never gets below 10% of the mean, after 30 realizations the 95% confidence interval is 10.7% of the mean drifting distance. However, the results indicate that the width of the numerical confidence intervals approaches convergence, after 20 realizations the confidence intervals are below 15% of the mean drifting distance, both when simulations are performed with the time-domain method and the Newman approximation.

For the drifting angle, 9 realizations with the time-domain method and 7 realizations with the Newman approximations are needed to get the 95% confidence intervals below 10% of the mean value, while 5 experimental realizations are needed to get the confidence interval below 10% of the mean.

Seo et al. (2019) performed a similar study with numerical simulations for the S175 hull. They concluded, for the S175 ship, that the variation around the mean value, converged after 15 repetitions. In general, it is difficult to conclude the exact number of realizations that are needed before the variation of the results converge. This will depend on the hull form and the sea states. However, it is reasonable to assume that between 10–20 realizations are needed before the 95% confidence intervals of the drifting distance and drifting angle are close to 15% of the mean value. In this context it is important to remember that the surface elevation is generated with deterministic amplitudes, i.e. the amplitude of each wave component in the spectrum is the same for every realization, while the phase angles are random. If the surface elevation was generated with amplitudes that were considered to be random variables, following a statistical distribution, it could be that the confidence intervals converge slower compared to using deterministic amplitudes.

The results in Figs. 22–23 illustrates the importance of considering the stochastic behavior when maneuvers in irregular waves are evaluated. If the drift loads are estimated with random surface elevation, one should be careful to conclude based on few repetitions.

5. Conclusion

A rational modular maneuvering model for maneuvering in regular and irregular waves is presented. A new model for the wave-modified inflow to the rudder is presented. For the x-component of the inflow, methods from the literature are applied. The y-component of the inflow is derived consistently with respect to the x-component. Sensitivity studies show that the effect of waves on the inflow velocities is most important for long waves.

The sensitivity to the variation of wave height during a turning circle in regular waves was investigated for a range of regular waves. Based on an extensive wave documentation of the wave environment during dedicated tests in the ocean basin at SINTEF Ocean, numerical simulations in a “virtual” basin, with varying wave height, were compared to simulations using constant wave height. For most responses there was no significant difference between these two simulation methods. However, for the drifting distance, in particular for the two longest waves, there was a significant difference between these two simulation methods. Overall, this implies that the variation of wave height in a basin contribute less to the uncertainty than expected.

The slowly varying second-order drift loads in irregular waves are calculated with two methods: The difference-frequency loads method using the Newman approximation, and a "time-domain" method where the incident wave elevation is decomposed into a series of individual waves, which are considered as regular waves. Both methods perform acceptable compared to experiments, for a range of sea states. However, the time-domain method performs in general slightly better than the method using the Newman approximation. One contribution to the difference can be that the difference-frequency method applies random phase angles, while the time-domain method uses the same wave elevation as the experiments. The most significant difference between the two methods is the computational time. In the current work, the time-domain method is 10–100 faster than the method using the Newman approximation. The drift loads calculated with the time-domain method, are for each wave encounter, proportional to the incident wave amplitude squared. This means that numerical inaccuracies, for specific encounter frequencies and/or wave headings, is magnified for extreme wave heights. This was recognized in the results, where some nonphysical peaks were observed for the sway velocity and yaw rate. It seems like the overall results are not affected by this behavior. However, this is something which needs further research. The slowly varying drift loads with the Newman approximation estimates the wave amplitudes, with contribution from all wave components in the wave spectrum, which results in a behavior that is less sensitive to individual large wave events.

New experimental free running maneuvering tests are presented for the DTC hull. Turning circles with 35° rudder angle were tested in regular and irregular waves. The experiments in irregular waves were performed for several time-windows for each wave spectrum. The variation of advance, tactical diameter, drifting distance, and drifting angle, due to different time-realizations of the wave spectrum was investigated both experimental and numerical. The 95% confidence intervals for advance and tactical diameter converges, to below 10% of the mean value, for less than 5 realizations. The drifting distance and drifting angle are more sensitive to number of realizations. Since maximum 10 experimental realizations were performed, it is not possible, based on the experiments, to conclude about the number of realizations for convergence of drifting distance and drifting angle. After 20 numerical realizations, the 95% confidence interval for drifting distance converges, to below 15% of the mean value. For the drifting angle, 9 realizations are needed to get the 95% confidence interval below 10% of the mean value.

CRediT authorship contribution statement

Øyvind Rabliås: Conceptualization, Methodology, Investigation, Data curation, Formal analysis, Software, Writing – original draft, Writing – review & editing. **Trygve Kristiansen:** Conceptualization, Formal analysis, Methodology, Writing – review & editing.

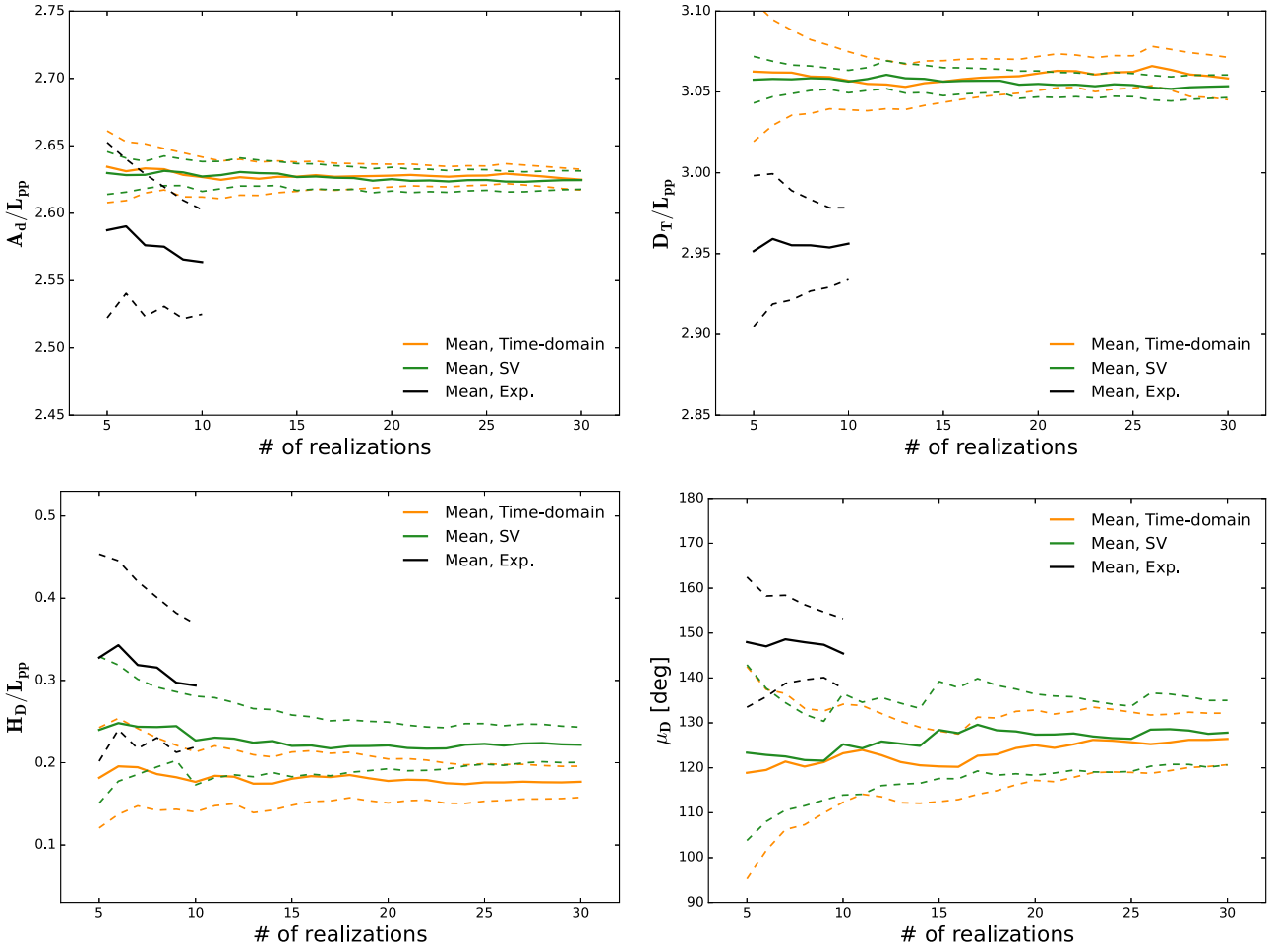

Fig. 23. Variation of advance, tactical diameter, drifting distance, and drifting angle as a function of number of realizations in the same sea state. H_s = 4.33 m and T_p = 13.96 s (WAVE ID 85030). Cumulative mean and 95% confidence intervals are presented. A maximum of 10 repetitions were run in our experiments. 30 numerical simulations are included to illustrate the rate of convergence. 95% confidence intervals are illustrated with dotted lines. Upper row: Advance and tactical diameter. Lower row: Drifting distance and drifting angle.

Declaration of competing interest

The authors declare that they have no known competing financial interests or personal relationships that could have appeared to influence the work reported in this paper.

References

Aung, M.Z., Umeda, N., 2020. Manoeuvring simulations in adverse weather conditions with the effects of propeller and rudder emergence taken into account. Ocean Eng. 197, 106857. http://dx.doi.org/10.1016/j.oceaneng.2019.106857.

Chillcce, G., el Moctar, O., 2018. A numerical method for manoeuvring simulation in regular waves. Ocean Eng. 170, 434–444. http://dx.doi.org/10.1016/j.oceaneng.2018.09.047.

Cura-Hochbaum, A., Uharek, S., 2016. Prediction of ship manoeuvrability in waves based on RANS simulations. In: 31st Symposium on Naval Hydrodynamics.

Faltinsen, O.M., Minsaas, K.J., Liapis, N., Skjørdal, S.O., 1980. Prediction of resistance and propulsion of a ship in a seaway. In: Proceedings of the 13th Symposium on Naval Hydrodynamics, Tokyo, 1980.

Fujii, H., 1975. Experimental study on the resistance increase of a ship in regular oblique waves. In: Proc. of 14th ITTC, 1975, Vol. 4. pp. 351–360.

Hsu, F., Blenkarn, K., 1972. Analysis of peak mooring forces caused by slow vessel drift oscillations in random seas. Soc. Pet. Eng. J. 12 (04), 329–344. http://dx.doi.org/10.2118/3256-pa.

ITTC, 2014. Uncertainty Analysis for Free Running Model Tests. Report, ITTC-Recommended Procedures and Guidelines.

el Moctar, O., Shigunov, V., Zorn, T., 2012. Duisburg test case: Post-panamax container ship for benchmarking. Ship Technol. Res. 59 (3), 50–64. http://dx.doi.org/10.1179/str.2012.59.3.004.

Nakamura, S., Naito, S., 1975. Propulsive performance of a container ship in waves. J. Soc. Naval Archit. Jpn. 15.

Newman, J.N., 1974. Second-order, slowly-varying forces on vessels in irregular waves. In: Proc. Int. Symp. Dynamics of Marine Vehicles and Structures in Waves. Mechanical Engineering Publications LtD.

Nguyen, V.M., Nguyen, T.T., Seo, J., Yoon, H.K., Kim, Y.G., 2018. Experimental Investigation of the Hydrodynamic Force Acting on Ship Hull and Rudder in Various Wave Direction. International Society of Offshore and Polar Engineers, p. 7.

Prpic-Orsic, J., Faltinsen, O.M., 2012. Estimation of ship speed loss and associated CO_2 emissions in a seaway. Ocean Eng. 44, 1–10. http://dx.doi.org/10.1016/j.oceaneng.2012.01.028.

Rabliås, Ø., Kristiansen, T., 2019. Free running maneuvering tests of the DTC hull in calm water and regular waves with focus on uncertainty analysis based on repetition tests. In: 5th MASHCON: International Conference on Ship Manoeuvering in Shaollow and Confined Water with Non-Exclusice Focus on Manoeuvering in Waves, Wind and Current. pp. 328–339.

Rabliås, Ø., Kristiansen, T., 2021. A 2D+t approach for the transverse viscous loads in a modular maneuvering model. Ocean Eng. 228, 108853. http://dx.doi.org/10.1016/j.oceaneng.2021.108853.

Salvesen, N., Tuck, E.O., Faltinsen, O.M., 1970. Ship motions and sea loads. Trans. SNAME 78 (8), 250–287.

Seo, M.-G., Kim, Y., 2011. Numerical analysis on ship maneuvering coupled with ship motion in waves. Ocean Eng. 38 (17), 1934–1945. http://dx.doi.org/10.1016/j.oceaneng.2011.09.023.

Seo, M.-G., Nam, B.W., Kim, Y.-G., 2019. Numerical evaluation of ship turning performance in regular and irregular waves. J. Offshore Mech. Arct. Eng. 142 (2), http://dx.doi.org/10.1115/1.4045095.

Skejic, R., 2008. Maneuvering and Seakeeping of a Single Ship and of Two Ships in Interaction (Ph.D. thesis).

Skejic, R., Faltinsen, O., 2006. A unified seakeeping and maneuvering analysis of a monohull in regular incident waves. In: Proceedings of the 7th International Conference on Hydrodynamics, Ischia. pp. 97–104.

Skejic, R., Faltinsen, O.M., 2013. Maneuvering behavior of ships in irregular waves. In: 32nd International Conference on Ocean, Offshore and Arctic Engineering. ASME, Volume 9: Odd M. Faltinsen Honoring Symposium on Marine Hydrodynamics, http://dx.doi.org/10.1115/OMAE2013-10169, 10.1115/OMAE2013-10169.

Sprenger, F., Fathi, D., 2015. D3.3 Report on Model Tests at MARINTEK. Report, (SHOPERA-D3.3).

Taskar, B., Yum, K.K., Steen, S., Pedersen, E., 2016. The effect of waves on engine-propeller dynamics and propulsion performance of ships. Ocean Eng. 122, 262–277. http://dx.doi.org/10.1016/j.oceaneng.2016.06.034.

Tello Ruiz, M., Mansuy, M., Delefortrie, G., Vantorre, M., 2019. Modelling the manoeuvring behaviour of an ULCS in coastal waves. Ocean Eng. 172, 213–233. http://dx.doi.org/10.1016/j.oceaneng.2018.11.046.

Ueno, M., Tsukada, Y., Tanizawa, K., 2013. Estimation and prediction of effective inflow velocity to propeller in waves. J. Mar. Sci. Technol. 18 (3), 339–348. http://dx.doi.org/10.1007/s00773-013-0211-8.

Wang, T., Ma, N., Gu, S., Feng, P., 2018. Effect of propeller thrust reduction on ship surfriding/broaching prediction. In: Proceedings of the 13th International Conference on the Stability of Ships and Ocean Vehicles, Kobe, Japan. pp. 109–118.

Yasukawa, H., Hirata, N., Matsumoto, A., Kuroiwa, R., Mizokami, S., 2018. Evaluations of wave-induced steady forces and turning motion of a full hull ship in waves. J. Mar. Sci. Technol. 1–15. http://dx.doi.org/10.1007/s00773-018-0537-3.

Yasukawa, H., Nakayama, Y., 2009. 6-DOF motion simulations of a turning ship in regular waves. In: Proceedings of the International Conference on Marine Simulation and Ship Manoeuvrability.

Yu, L., Wang, S., Ma, N., 2021. Study on wave-induced motions of a turning ship in regular and long-crest irregular waves. Ocean Eng. 225, 108807. http://dx.doi.org/10.1016/j.oceaneng.2021.108807.

Zhang, W., Zou, Z., 2016. Time domain simulations of the wave-induced motions of ships in maneuvering condition. J. Mar. Sci. Technol. 21 (1), 154–166. http://dx.doi.org/10.1007/s00773-015-0340-3, Df4cd Times Cited:1 Cited References Count:23.